Received: 1 November 2017 | Revised: 16 July 2018 | Accepted: 25 August 2018

DOI: 10.1111/bre.12314

ORIGINAL ARTICLE

WILEY Basin Research IAS EAGE

Resolving the contributing factors to Mississippi Delta subsidence: Past and Present

Bruce C. Frederick[1] | **Michael Blum**[1] | **Richard Fillon**[2] | **Harry Roberts**[3]

[1]Department of Geology, University of Kansas, Lawrence, Kansas

[2]Earth Studies Group, Punta Gorda, Florida

[3]Department of Oceanography and Coastal Sciences, Coastal Studies Institute, Louisiana State University, Baton Rouge, Louisiana

Correspondence
Bruce C. Frederick, Department of Geology, University of Kansas, Lawrence, KS.
Email: bruce.c.frederick@gmail.com

Funding information
Ritchie Distinguished Professorship in the Department of Geology, University of Kansas

Abstract

To date, quantification of individual components that contribute to shallow and deep-seated subsidence in passive margin deltas worldwide has proven problematic. A new, regional gridded chronostratigraphic dataset for the Lower Mississippi Delta region, derived from 80,928 well reports across the northern Gulf of Mexico (GOM), has bridged the disparity between geodetic mean rates measuring total land surface subsidence across annual-to-decadal timescales and the deep-seated stratigraphic subsidence rates that record isostatic response over timescales of $>10^4$ years. Through a quantitative assessment of gridded chronostratigraphic surfaces, sections, and subsidence rates extending from the Middle Pleistocene (0.58 Ma) to the Late Pliocene (3.85 Ma), we identify both temporal and spatial variability in deep-seated subsidence across the northern GOM. Targeted deep-seated subsidence data extracted across prior GOM Holocene sea-level sample locations have revealed more than an order of magnitude greater rates of isostatic compensation in the Mississippi depocentre versus similar GOM sea-level control sites in Florida and Alabama, casting doubt on efforts towards a representative Holocene sea-level curve. Spatial variability in subsidence was also assessed locally in both the strike and dip directions to assess the contributions of growth faults. Fault throw displacement magnitude was discovered to decrease with depth, accounting for less than half of the total deep-seated subsidence record of the Middle Pleistocene. Temporal subsidence complexities were also revealed including a direct, inverse logarithmic relationship between subsidence rate and time indicating variable subsidence component controls across different timescales. Despite the spatial and temporal complexities, this dataset serves as the first regional baseline for deep-seated subsidence rates across the northern GOM.

1 | INTRODUCTION

Worldwide, passive margin river delta regions remain vertically challenged with land surface elevation inherently tied to the balance between rates of eustatic sea-level change, sediment supply deposition, and subsidence. Cities and other large population centres across the globe have rapidly exploited the incredibly flat (0.0001 m/m), fertile soils of fluvio-deltaic depocentres with their characteristically abundant fresh water supply and productive estuaries (Syvitski & Saito, 2007). With more than 634 million persons globally residing on delta plains and other low elevation coastal zones (McGranahan, Balk, & Anderson, 2007), accurate quantification of delta region land surface dynamics across

historical and geologic timescales is paramount. In this paper we summarise the components of land surface subsidence and relative sea-level (RSL) rise, quantify deep-seated subsidence rates and highlight the spatial and temporal complexities of coastal land loss across a depocentre associated with the fourth largest drainage basin in the world (Syvitski & Milliman, 2007) and a coastal zone population exceeding two million (Batker et al., 2012).

Coastal land loss in the Mississippi River delta region of southern Louisiana is well documented and results from the combined effects of land-surface subsidence, sediment deficits and global sea-level rise (Blum & Roberts, 2009, 2012; Blum, Tomkin, Purcell, & Lancaster, 2008; Karegar, Dixon, & Malservisi, 2015; Kulp, 2000; Meckel, ten Brink, & Williams, 2006; Törnqvist et al., 2008; Wolstencroft, Shen, Törnqvist, Milne, & Kulp, 2014). Subsidence rates over historic periods have been estimated at ~10 mm/year, with extreme values reported at 29–66 mm/year (Dixon et al., 2006; Dokka, 2011; Dokka, Sella, & Dixon, 2006; Jankowski, Törnqvist, & Fernandes, 2017; Karegar et al., 2015). With current global sea-level rise exceeding 3 mm/year (Cazenave & Llovel, 2010; Cazenave et al., 2014; Church et al., 2013), rates of RSL rise are presently estimated at 12.0 ± 8.3 mm/year across the Mississippi Delta and Chenier Plain (Jankowski et al., 2017). Land-surface subsidence is dominated by compaction and dewatering of Holocene deltaic sediments primarily focused within the uppermost 5–10 m of strata (Jankowski et al., 2017), but must also include a deep-seated component that reflects growth faulting, lithospheric flexure, long-term compaction and fluid extraction that has a much larger depocentre-scale footprint. Largely because these deep-seated subsidence component rate magnitudes have long been estimated to be nominal, relative to the shallow compaction component (Blum & Roberts, 2012), their deep-seated subsidence contribution has remained poorly constrained.

This paper presents a quantitative assessment of deep-seated subsidence rates and their variability in space and through time. Here we deploy a dataset of biostratigraphic picks extending back to 3.85 Ma that define eight Late Pliocene to Middle Pleistocene depositional surfaces defining chronostratigraphic sequences from 80,928 subsurface well penetrations across the northern Gulf of Mexico (GOM) to map the depth and thickness of individual stratigraphic intervals, we then invert this record to calculate subsidence rates and their spatial and temporal variability. Our study area extends (a) north-to-south from the exposed Pleistocene Prairie Formation outcrops of the Lower Mississippi River Valley to the modern-day shelf margin in water depths of <100 m (Figure 1); and (b) in the east-to-west direction from the Florida panhandle to east Texas. In addition to quantifying spatial variability in deep-seated subsidence, we also compare longer and shorter term rates to illustrate an inverse relationship with time interval over which they are calculated similar to measurement interval bias originally described by Sadler (1981).

Highlights

- Deep-seated subsidence rates for the Lower Mississippi Delta reveal isostatic response over 10^4–10^7 years
- Temporal and spatial variability in deep-seated subsidence rates detailed across the northern GOM
- Spatial isostatic compensation variability calls into question previous Holocene sea level research
- Inverse logarithmic temporal deviations indicative of disparate subsidence component controls

2 | BACKGROUND

Subsidence research in the Mississippi River delta region has proceeded with renewed vigour following the flooding associated with Hurricanes Rita and Katrina in 2005, and the increased recognition of coastal land loss (Blum & Roberts, 2009; González & Tornqvist, 2006; Penland & Ramsey, 1990; Törnqvist, Bick, van der Borg, & de Jong, 2006). Land-surface subsidence represents the integration of a number of geologic processes that operate at different depths, and over different spatial-temporal scales (Kulp, 2000). Longer term geologic processes operating below the Pleistocene-Holocene stratal contact are inherent to the Mississippi deltaic depocentre and represent the primary driver for regional deep-seated subsidence including pre-Holocene compaction, glacio-isostatic forebulge collapse, Holocene sedimentary isostatic adjustment, and growth fault movement. In particular, there has been ~200 km of north-to-south Neogene and Quaternary deltaic and shelf-margin progradation, extending east-to-west from

FIGURE 1 Extent of study region and generalized geologic map of lower Mississippi River valley, delta region, and Gulf of Mexico coast illustrating shelf-margins positions and mapped growth faults (McCulloh & Heinrich, 2013; Murray, 1961). Pleistocene alluvial-deltaic deposits are shown in orange, whereas Holocene strata are shown in yellow. Sites where published Holocene sea-level records have been defined are shown by coloured symbols, as indicated in the figure legend. PTA refers to the first occurence of Trimosina A micropalaeontological datum

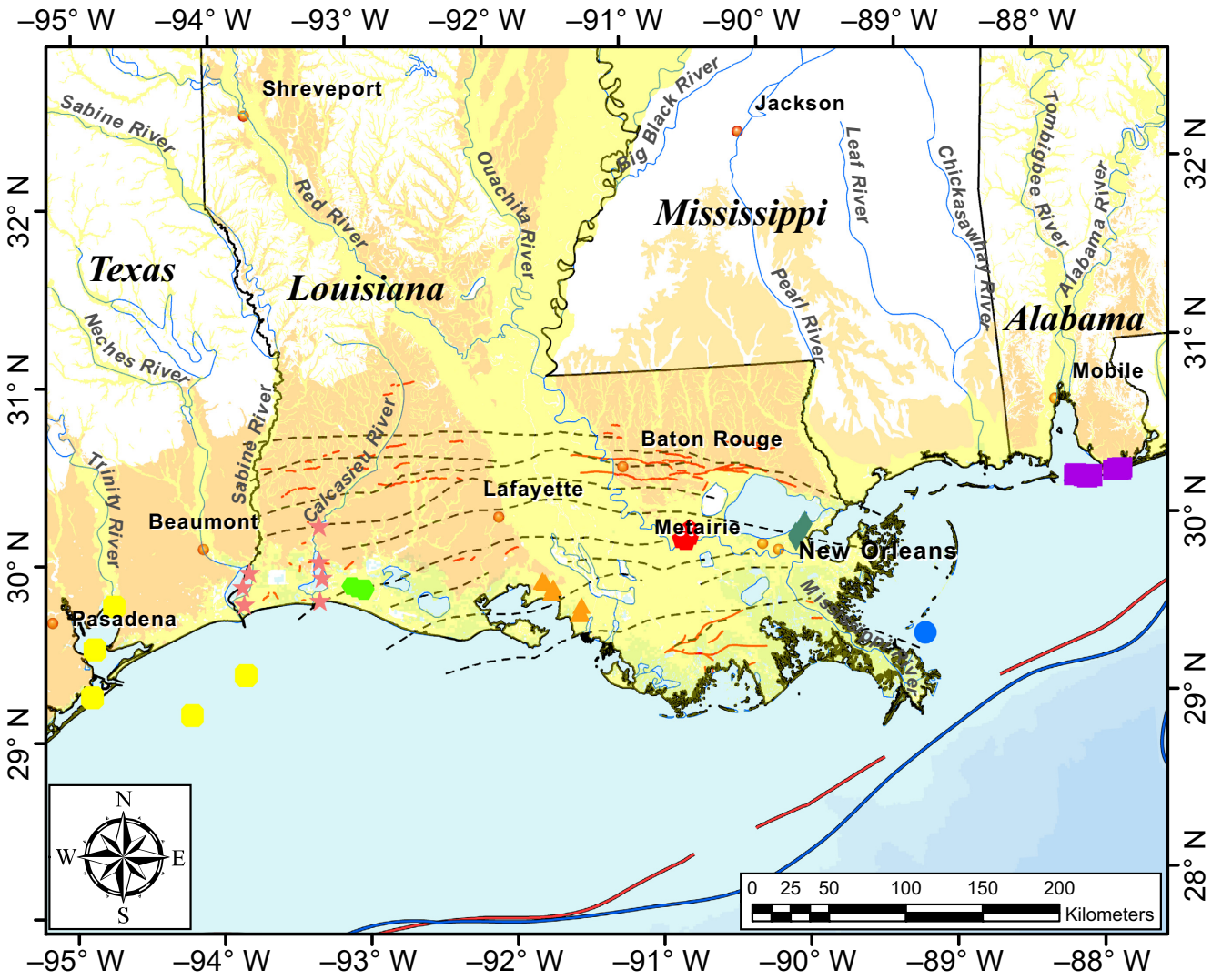

Blum et al (2003) - AL Sample Locations
Edrington et al (2008) - LA Sampling Locations
Milliken et al (2008) Sample Locations
Rodriguez et al (2004-2005) Sample Locations
Straub et al (2009) Sample Locations
Tornqvist et al (2004) - Lutcher-Gramercy Sample Locations
Tornqvist et al (2006) - Bayou Cypremort-Sale Sample Locations
Yu et al (2012) - Chenier Plain Sample Locations
Holocene Shelf Margin
Pleistocene (PTA) Shelf Margin
McCulloh & Heinrich (2013) Faults
Murray (1961) Faults

Mississippi to the Louisiana-Texas border. Moreover, Late Tertiary and Quaternary fluvial to shallow-marine sediments are >500 m thick at the latitude of New Orleans, increasing to >4,000 m at the shelf margin (McFarlan & LeRoy, 1988; Woodbury, Murray, Pickford, & Akers, 1973).

Continuously operating GPS reference stations have collected measurements over the last few decades throughout the Gulf Coastal region (Dokka et al., 2006; Karegar et al., 2015). Regression of GPS data from the delta region suggests uplift of <1 mm/year to the north, east, and west of the Holocene alluvial-deltaic plain, a hinge-line at the latitude of Baton Rouge (N 30.5°) where subsidence goes to zero, and an increase to >11 mm/year through the lower delta plain (Blum & Roberts, 2012; Jankowski et al., 2017; Karegar et al., 2015). This pattern of north-to-south subsidence rate increase parallels Neogene to Quaternary patterns of sediment loading. GPS reference stations provide the most precise subsidence rate data available for modern subsidence rates because they are calibrated to the geoid and independent of other measures. However, monuments for GPS instruments are grounded 15–36 m below the surface within the area of thick Holocene alluvial-deltaic strata (Dokka et al., 2006) with subsidence rate measurements only providing a minimum rate for land-surface subsidence (Blum & Roberts, 2012) without distinction between subsidence mechanisms operating at different depths.

For the discussion that follows, we consider the shallow component of land-surface subsidence to reflect dewatering and compaction of Holocene mud- and organic-rich alluvial-deltaic strata, and the deep-seated component to reflect processes that operate below the Pleistocene-Holocene stratal contact including compaction of pre-Holocene strata, isostatic response to long-term sediment loads, growth faults, salt tectonics, and glacio-isostatic forebulge collapse (Diegel, Karlo, Schuster, Shoup, & Tauvers, 1995; Galloway, 2008; Kulp, 2000; Peel, Travis, & Hossack, 1995; Yu, Törnqvist, & Hu, 2012; Yuill, Lavoie, & Reed, 2009). Shallow subsidence processes comprise the majority (with estimates upwards of 90%) of land-surface subsidence as a whole (Jankowski et al., 2017; Meckel et al., 2006; Penland & Ramsey, 1990; Roberts, Bailey, & Kuecher, 1994; Törnqvist et al., 2008), but the deltaic depocentre could not have developed without accommodation generated by long-term subsidence of significant magnitude (Blum & Roberts, 2012).

Despite the overwhelming evidence of long-term deltaic subsidence, deep-seated subsidence components and associated processes have remained poorly constrained. On one end of a spectrum, Dokka et al. (2006) argued that geodetic rates of 15–25 mm/year during the 1970s in the eastern part of New Orleans indicated movement on large growth faults, which were suggested to be a major contributor to subsidence. However, subsequent structural and stratigraphic research reveal very little fault offset at the Pleistocene-Holocene stratal contact that would support interpretations of higher long-term rates in New Orleans parish area with time-averaged middle Miocene to present subsidence rates of <0.2 mm/year (Edrington, Blum, Nunn, & Hanor, 2008; Straub, Paola, Mohrig, Wolinsky, & George, 2009). These results increase the probability that the extreme geodetic rates captured in Dokka et al. (2006) represent transient phenomena, including potential growth fault movement driven by groundwater withdrawal, and are not representative of deep-seated rates in general (Dokka, 2011; Jones et al., 2016). A more recent detailed study of the Baton Rouge-Tepetate fault system by Shen et al. (2017) supports this view, confirming that fault throw rates vary over time, which they attribute to glacial-interglacial shifts in the location of active deltaic deposition, but aggregate late Holocene throw rates were <0.7 mm/year.

On the other end of the spectrum, Törnqvist et al. (2006) present records of RSL from radiocarbon-dated basal peats along the Pleistocene-Holocene stratal contact within the Holocene alluvial-deltaic plain. They argue that the similarity of composite RSL records from Mississippi Delta region, including the western and eastern margins of the Holocene valley, with the composite sea level record from the tectonically stable Caribbean region indicate minimal differential lithospheric subsidence across the study area supporting the hypothesis of a near stable Pleistocene-Holocene stratal contact subsiding at 0.25 mm/year or less. A number of researchers subsequently modelled isostatic response to Holocene sediment loading (Blum et al., 2008; Wolstencroft et al., 2014) to show that isostatic effects from Holocene loading are small (mostly between 0.5–2 mm/year), but cannot be zero, and the Pleistocene-Holocene stratal contact cannot be vertically stable. The Törnqvist et al. (2006) view was subsequently modified by Yu et al. (2012), based upon basal peat records from the Chenier Plain, to the west of the Holocene valley fill and delta plain, where differential rates of 0.15 mm/year were calculated between the Chenier Plain and the Holocene delta plain sites in Törnqvist et al. (2006). Yu et al. (2012) concluded that the effects of sediment loading are therefore real, but rates are about an order of magnitude smaller than recent studies had postulated (see also Wolstencroft et al., 2014).

Spatial variability in relative vertical motion for the Pleistocene-Holocene stratal contact is one part of the deep-seated subsidence record, but it is important to recognise that all basal-peat study sites, including those in Törnqvist et al. (2006) and Yu et al. (2012), reside within the larger Neogene and Quaternary deltaic depocentre. In this context, the issue of deep-seated subsidence is embedded in discussions about GOM middle to late Holocene RSL and its spatial variability (Blum et al., 2008; Donnelly & Giosan, 2008). For example, Törnqvist et al. (2004, 2006)

interpret age-depth relationships of basal peats in the delta region to indicate continual submergence at rates of <1 mm/year since ca. 6 Ka. Because they assume the Pleistocene-Holocene stratal contact is near stable with subsidence rates of <0.25 mm/year, this record is argued to represent GOM sea-level change as a whole with continual submergence driven by glacio-isostatic forebulge collapse (Törnqvist et al., 2004; Yu et al., 2012). The primary controversy revolves around interpretations of RSL records from sites that are far from the deltaic depocentre. On the one hand, Morton, Paine, and Blum (2000) and (Blum, Carter, Zayac, & Goble, 2002; Blum, Sivers, Zayac, & Goble, 2003; Blum et al., 2001) argue that middle to late Holocene coastal landforms along the Texas and Alabama coasts record relative sea-level positions that were 1–2 m higher than present day, whereas Blum et al. (2008) interpret the differences between these sites and the Mississippi Delta to represent spatially variable isostatic effects that are intrinsic to a coastline with a large deltaic depocentre. By contrast, studies by Rodriguez and Meyer (2006) in Alabama, Milliken, Anderson, and Rodriguez (2008) in east Texas, and Simms, Lambeck, Purcell, Anderson, and Rodriguez (2007) in south Texas interpret continual submergence consistent with the González and Tornqvist (2006) record from the Mississippi Delta region. Taking these interpretations at face value, the same record of RSL in these different areas would indicate either that there is no deep-seated subsidence, that all of the sites have the same deep-seated subsidence history, or that there is a coincidental convergence of results from different processes (Blum et al., 2008).

Understanding the rates and spatial variability of deep-seated subsidence components is therefore not only central to understanding the spatial and temporal variability of the absolute subsidence record as a driver for coastal land loss in the Mississippi Delta region, but also critical to the reconciliation of different interpretations of the northern GOM RSL record. Our study presents the first regional evaluation of deep-seated subsidence rates across the northern GOM.

3 | METHODS

Here we access a proprietary industry database of Late Neogene and Quaternary biostratigraphic picks from 80,928 wells across the GOM to quantitatively assess the magnitude and spatial-temporal variability of deep-seated subsidence (Figure 2). An overview of the biostratigraphic database can be found in Supplemental Information herein (Fillon, 2016) or at: https://www.paleodata.com/wp-content/uploads/2017/08/GOM-Deposystem-Database-Overiew_2017.pdf. Chronologically controlled stratigraphic picks were compiled from the first down-hole occurrence (i.e., last appearance datum) of a micropalaeontological datum relative to the WGS84 geoid approximation of mean sea level, in onshore and offshore wells using *Stratrate*, a correlation software package that employs a three-step methodology to populate a geodatabase. This approach is grounded on: (a) initial assignment of ages and confidence rankings to the first downhole appearance (i.e., last appearance datum) of known microfauna and flora, and formation tops; (b) calculation of geohistory curves and removal of conflicting tops of lowest rank ("residuals"); and (c) statistical examination of the residuals and conservative age adjustments including confidence ranking to produce a total composite database of 77 Palaeozoic to Quaternary chronostratigraphic surfaces termed "chronosequences" from >225,000 wells. Data from the eight uppermost chronosequences representing the Late Pliocene (3.85 Ma) through the Middle Pleistocene (0.58 Ma) are presented herein (Table 1). Additional chronostratigraphic methodology and well location detail is provided as Supplementary Information. Each gridded chronosequence surface, depicting the first downhole occurrence of a micropalaeontological datum, inherently defines a marine transgressive surface that may also chronologically constrain a more regionally significant maximum flooding surface (MFS).

Every chronosequence top was gridded at 0.03° latitude by 0.03° longitude, over an area that extends from the coastal plain to the palaeo-shelf margin, using bi-linear interpolation of grids derived from minimum curvature. The minimum curvature algorithm most accurately emulates the very low-relief topographic and bathymetric contours generated in fluvial-deltaic depositional environments, because it fits the smoothest possible surface by initially calculating the gross average value of the data within the input constraints, identifying the number of nodes needed to represent the regional trend and then performing successive iterations to calculate additional grid nodes to incorporate local features. Gridded maps of subsidence rates were then generated in similar fashion for each chronosequence top by dividing elevations by their respective ages. In doing so, we assume the gridded surface represents an interglacial period delta plain shoreline to inner shelf depositional surface with an elevation similar to that of the Holocene: for example, over the Plio-Pleistocene, the last 4 Ma, interglacial highstand elevations that define our chronosequence tops are within ±~30 m of present elevations (e.g., Miller, Mountain, Wright, & Browning, 2011; Miller et al., 2005) (Figure 3a; Table 1). These Plio-Pleistocene interglacial highstand elevations (Miller et al., 2005), generated from backstripping-related errors potentially including hiatuses, palaeowater depths, and deposystem topography on a 10^6-year timescale, are generally an order of magnitude smaller than the burial depths of the respective chronostratigraphic boundaries with uncertainties falling between ±10 and 50 m of estimated sea level. We

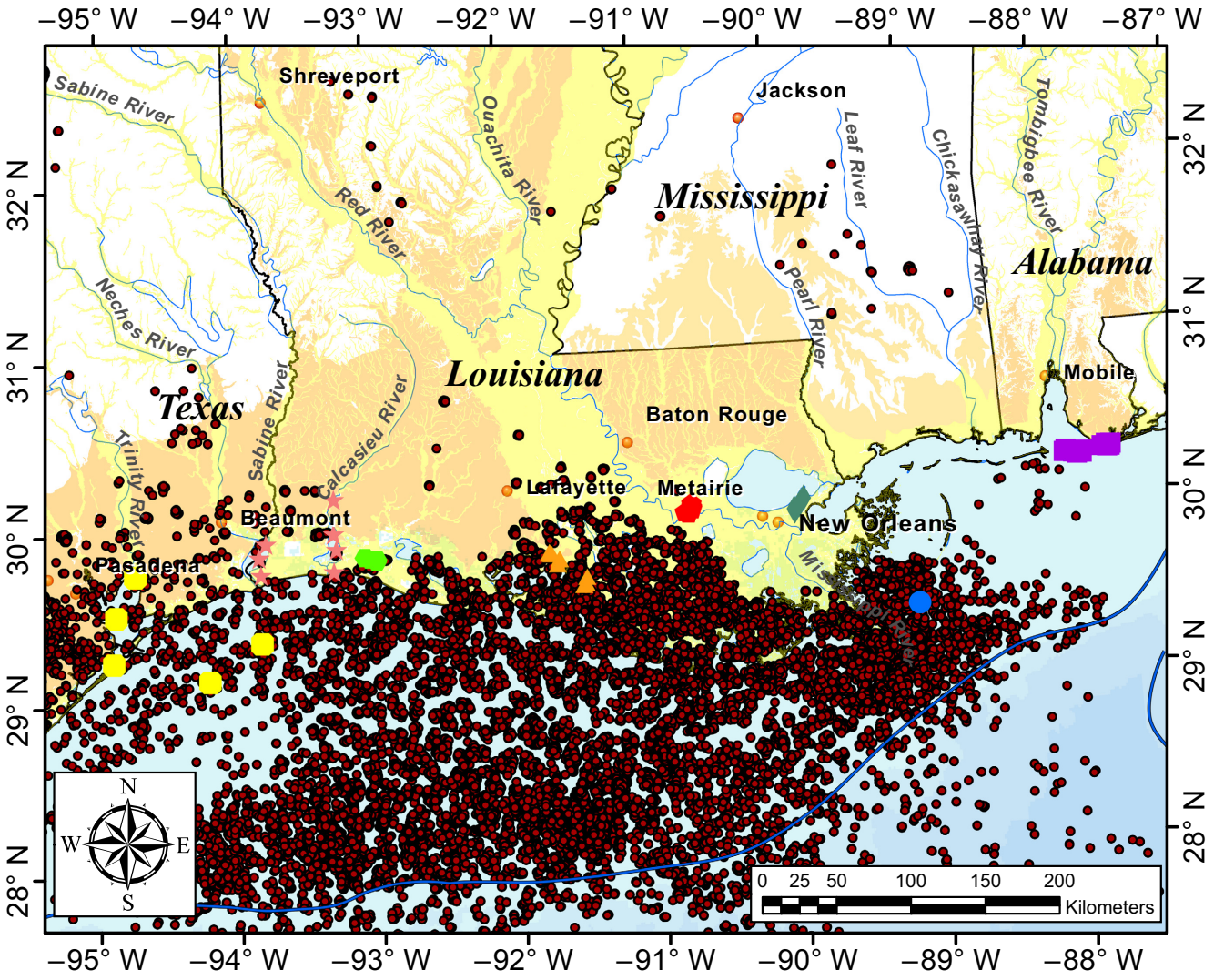

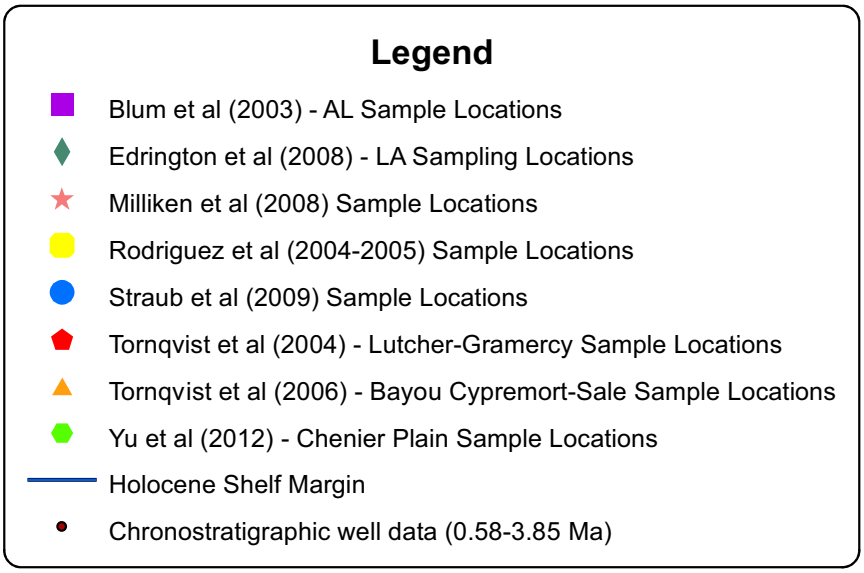

FIGURE 2 Extent of study region and generalised geologic map of lower Mississippi River valley, delta region, and Gulf of Mexico coast illustrating Holocene shelf-margins position and 80,928 chronostratigraphic well datapoints extending from 0.58–3.85 Ma. Pleistocene alluvial-deltaic deposits are shown in orange, whereas Holocene strata are shown in yellow. Sites where published Holocene sea-level records have been defined are shown by coloured symbols, as indicated in the figure legend above. Despite an abundance of wells in the Greater New Orleans area, regrettably, most do not display palaeo events in the Plio-Pleistocene

TABLE 1 Summary of Plio-Pleistocene Gulf of Mexico Chronostratigraphic Surfaces (Chronosequences 1–8) used in this study based upon the first statistically significant downhole occurrence of micropalaeontological data from 80,928 wells (e.g. the first downhole occurrence of *Emiliania huxleyi* would be 0.58 Ma)

Gulf of Mexico chronostratigraphic surfaces				
Chronosequence number	Ages (Ma)	Miller et al. (2005) Sea-level elevation (m)	Epoch	Biostratigraphic indicator species
1	0–0.58	−25.6	Middle Pleistocene to Holocene	*Emiliania huxleyi*
2	0.58–1.02	−27	Early to Middle Pleistocene	*Pseudoemilania lacunosa*
3	1.02–1.22	−47.2	Early Pleistocene	*Large Gephyrocapsa*
4	1.22–1.63	−38.4	Early Pleistocene	*Helicosphaera sellii*
5	1.63–1.93	−16.8	Early Pleistocene	*Calcidiscus macintyrei*
6	1.93–2.39	24.8	Early Pleistocene	*Discoaster brouweri*
7	2.39–3.13	−10.5	Late Pliocene to Early Pleistocene	*Discoaster tamalis*
8	3.13–3.85	7.2	Early to Late Pliocene	*Dentoglobigerina altispira IZ*

These markers are generally referred to as "tops," because they mark the tops of regionally or locally correlative intervals represented by the highest occurrences of index taxa or lithologic change encountered by the drill bit. Miller et al. (2005) sea-level elevations reflect heights associated with chronosequence marker "tops." Biostratigraphic indicator species and associated ages based on the work of Fillon (2016) and the Geologic Time Scales published by Ogg, Ogg, and Gradstein (2016) and Gradstein, Ogg, Schmitz, and Ogg (2012).

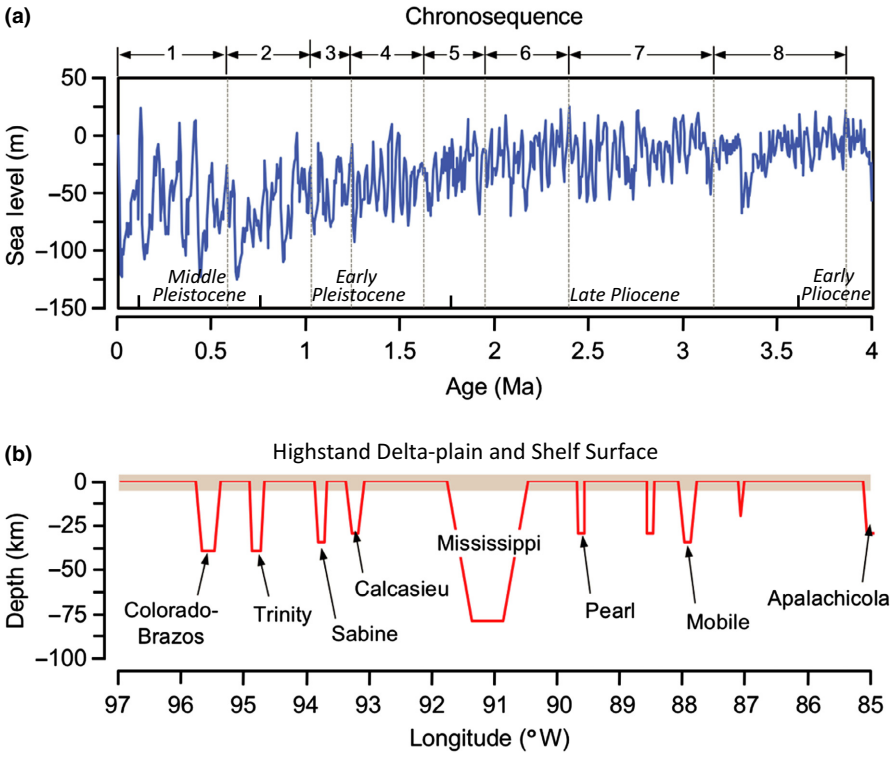

FIGURE 3 (a) Miller et al. (2005) Global Sea Level Curve highlighting the waxing and waning of the Northern Hemisphere ice sheet during the Pliocene-Holocene paced by 10^4–10^4 year scale Milankovich changes. These $\delta^{18}O$ records also show a dominant 100 Kyr eccentricity cycle and a secondary 41 Kyr obliquity phased wavelength, and (b) Interglacial highstand surfaces dissected by glacial period valleys. Incised valley model depicts depth estimates for first potential downhole stratigraphic indicator

also assume that interglacial highstand surfaces are dissected by subsequent glacial period incised valleys, which result in considerable erosional relief on these chronosequence tops (Figure 3b). The assumption of glacial period valley erosion of interglacial highstand surfaces is especially pertinent when examining data in the coast-parallel direction.

A number of additional potential uncertainties can also be identified relative to the chronostratigraphic methodologies employed herein. First, there is a decreasing density of biostratigraphic data moving onshore and up through the stratigraphic succession because of decreasing industry interest in the core and well cuttings from which biostratigraphic data are derived. As a result, the Plio-Pleistocene is

constrained by fewer datapoints (80,928) compared to the Neogene as a whole (>225,000). Back-stacking methodology (Fillon, 2007) based on subtracting chronosequence isopachs from the ETOPO5 global land surface-seabed digital elevation model (NOAA data announcement 88-MGG-02) is used to compile stratigraphic elevations below the topographic/bathymetric surface (See Supplemental Information for additional detail). Although the potential for current surface relief to strongly influence the back-stacked chronosequence surfaces exists, it is evident (Figure 4) that the generally flat surface relief of the Gulf Coastal Plain minimises this source of error. Therefore, we deem the reconstructed Plio-Pleistocene chronosequence surfaces used herein to reliably track deep-seated subsidence across the region. In this study, we focus principally on subsidence rates which are a calculated derivative of chronosequence thickness, and therefore completely independent of current surface relief. Subsidence rate patterns for Late Neogene (3.85–0.58 Ma) chronostratigraphic sequences offer many useful insights into the spatial and temporal variability of subsidence mechanisms operating at different depths. Although the resolution of the derived subsidence data is affected by the relative scarcity of biostratigraphic data available in the Upper Plio-Pleistocene sections of wells, compared to deeper intervals, the data quality and density are considered sufficient to track both spatial and temporal variations within the region (Figure 2).

Strike- and dip-oriented cross sections of chronosequence top elevations and subsidence rates were subsequently generated for every 0.25° of latitude from 28.5 to 30.5°N, and every 0.5° of longitude from −92.5 to −89.5°W, respectively, across the Mississippi deltaic depocentre (Figure 1): here, our focus is on the Plio-Pleistocene only (<3.85 Ma). Strike- and dip-oriented cross sections were then examined at multiple scales to assess regional subsidence patterns stemming from lithospheric flexure and deep-seated compaction, which drives larger scale patterns, as well as contributions from more localised movement on growth faults. Depths and subsidence rates were also digitally extracted along the northern GOM coastline, from Corpus Christi, Texas to Apalachicola, Florida, through locations where interpretations of Holocene sea-level change have been published. These data are used to illustrate alongshore variability in deep-seated subsidence rates, as they pertain to reconstructions of sea-level change.

Irrespective of the regional dip of each chronosequence surface, fault throw rates were calculated by detailing the vertical displacement difference at chronosequence local maxima versus local minima along dip-oriented cross sections and dividing by the representative chronostratigraphic datum at each fault plane intersection based upon the work of McCulloh and Heinrich (2013) and Murray (1961). Given the natural curvature of the growth fault plane in the subsurface, most pronounced in map view, there exists potential for these displacement results to represent more conservative oblique offset measurements between hanging wall maxima and footwall minima.

4 | RESULTS

4.1 | Depths chronosequence tops and sediment thicknesses

Strike-oriented cross sections extracted along the present-day coastline from Texas to Alabama display the general magnitude, timing, and spatial variability of sediment thicknesses across the northern GOM (Figure 4). The primary sedimentary sequence thickness at this regional scale extends from −90 to −93°W, and defines the long-term position of the Mississippi River sediment fairway and depocentre. A secondary fluvio-deltaic sedimentary sequence can be identified to the west, from western Louisiana to east-central Texas, and reflects deposition by the smaller Trinity, Brazos, and Colorado Rivers of the Texas coast, with minimal comparative sediment thicknesses occur to the east of −89.5°W in Mississippi, Alabama, and Florida.

Superimposed on this regional pattern, all strike-oriented chronostratigraphic surfaces reveal significant thickness variability at an along-strike scale of 10's of kilometers, which we interpret to represent incision associated with palaeovalleys, as illustrated in Figure 3b. Incisional morphologies are characterised by the anomalously deep appearances of biostratigraphic tops on a local basis, with the deepest of these being of the same scale as the last glacial period Mississippi valley (e.g., Blum & Roberts, 2012), and generally centred at −91.8°W, within the middle of the primary sediment thick. Other smaller scale

FIGURE 4 Generally strike-oriented cross sections of chronosequence tops, based on extraction of chronostratigraphic data along the Gulf of Mexico shoreline and through published Holocene sea-level study locations. Fault symbol locations (–▪–) indicate where this line crosses growth faults, as mapped in Murray (1961). Letters represent sea-level change study locations: A = Rodriguez, Anderson, Siringan, and Taviani (2004) and Rodriguez, Anderson, and Simms (2005), B = Milliken et al. (2008), C = Yu et al. (2012), D = Törnqvist et al. (2006), E = Törnqvist et al. (2004), F = Edrington et al. (2008), G = Blum et al. (2003). Spontaneous potential (SP) electric logs from adjacent wells are displayed where available for stratigraphic control. Note: Onshore depths and calculated subsidence rates at incised valley locations (e.g. ~−91.8 and ~−86.75°W) may be subject to down-stacking and Plio-Pleisotcene data scarcity bias

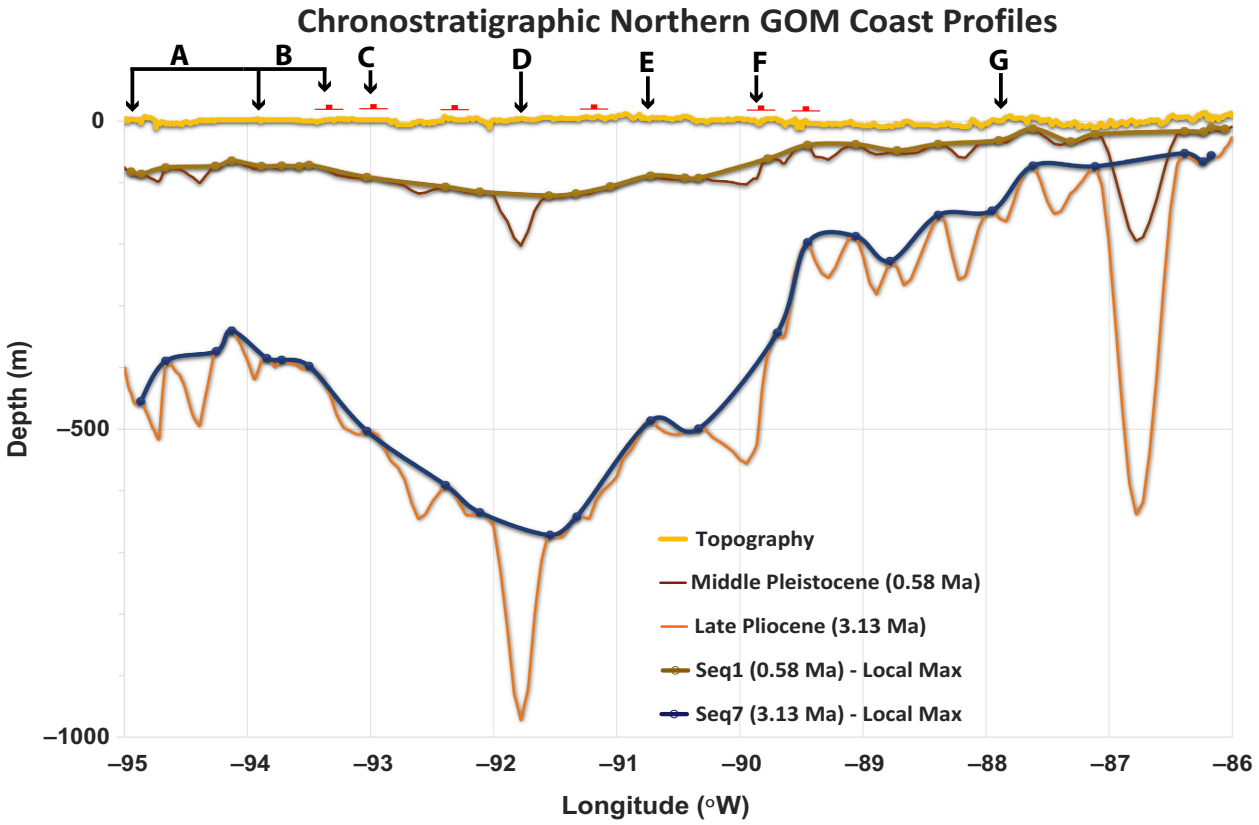
Chronostratigraphic Northern GOM Coast Profiles
A
B
C
D
E
F
G
0
−500
−1000
Depth (m)
−95
−94
−93
−92
−91
−90
−89
−88
−87
−86
Longitude (°W)
Topography
Middle Pleistocene (0.58 Ma)
Late Pliocene (3.13 Ma)
Seq1 (0.58 Ma) - Local Max
Seq7 (3.13 Ma) - Local Max

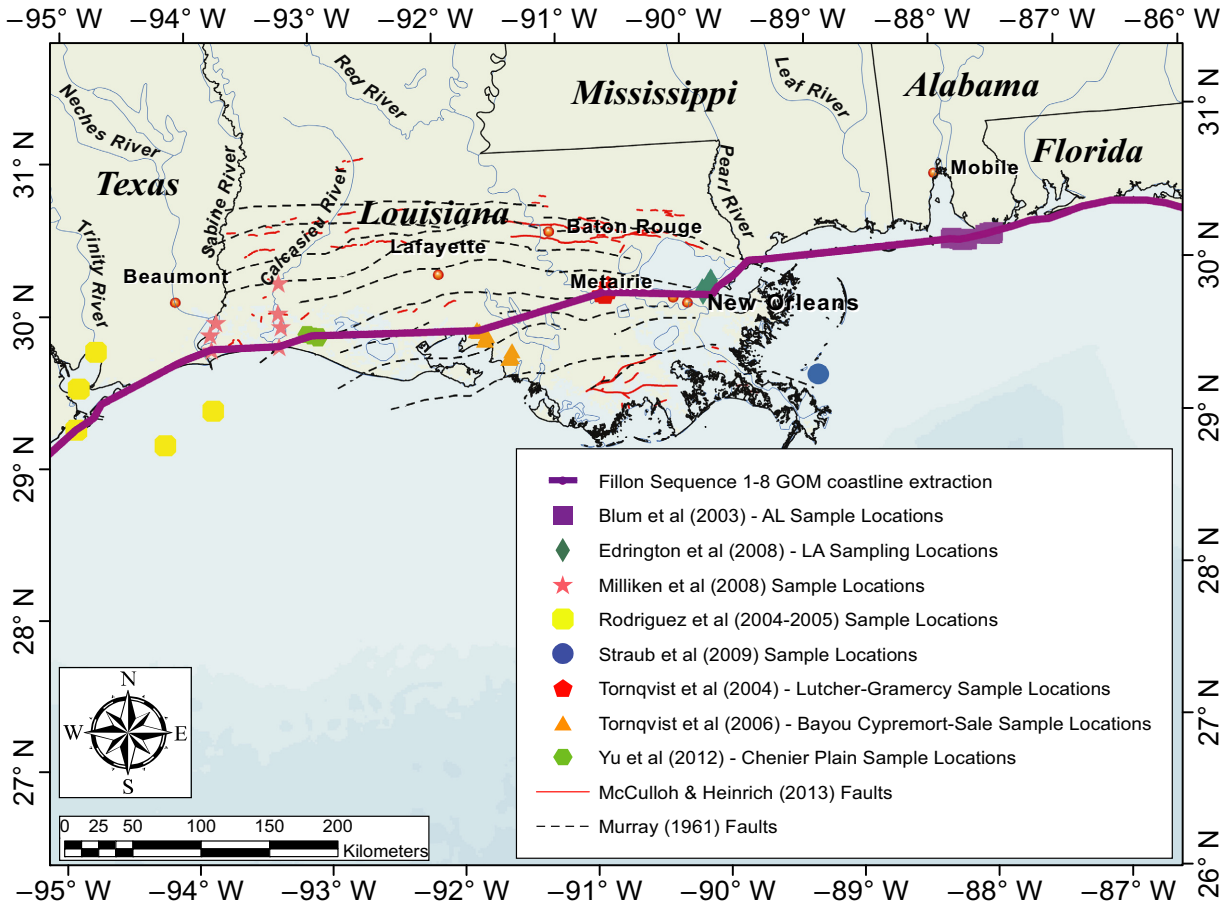
−95° W
−94° W
−93° W
−92° W
−91° W
−90° W
−89° W
−88° W
−87° W
−86° W
31° N
30° N
29° N
28° N
27° N
26° N
Mississippi
Alabama
Florida
Texas
Louisiana
Red River
Leaf River
Neches River
Sabine River
Calcasieu River
Pearl River
Trinity River
Mobile
Baton Rouge
Lafayette
Beaumont
Metairie
New Orleans
Fillon Sequence 1-8 GOM coastline extraction
Blum et al (2003) - AL Sample Locations
Edrington et al (2008) - LA Sampling Locations
Milliken et al (2008) Sample Locations
Rodriguez et al (2004-2005) Sample Locations
Straub et al (2009) Sample Locations
Tornqvist et al (2004) - Lutcher-Gramercy Sample Locations
Tornqvist et al (2006) - Bayou Cypremort-Sale Sample Locations
Yu et al (2012) - Chenier Plain Sample Locations
McCulloh & Heinrich (2013) Faults
Murray (1961) Faults
N
W
E
S
0 25 50 100 150 200
Kilometers

incisional morphologies are comparable in magnitude to depths of palaeovalleys from smaller GOM rivers (Martin, Cantelli, Paola, Blum, & Wolinsky, 2011), and generally located in a position that is consistent with those palaeovalleys. To provide representative minimum depths and corresponding sediment thicknesses along-strike for each chronosequence, we minimise the variability associated with palaeovalleys by smoothing across incisional features. As shown in Figure 4, these smoothed profiles reveal Plio-Pleistocene thicknesses (sum of Chronosequences 1–7, the last ~3.1 Ma) that range from <100 m in Alabama and the Florida panhandle, to ~350 m along the east Texas coast, to >650 m under the present Mississippi Delta plain in south Louisiana. Corresponding values for the middle Pleistocene to present (Chronosequence 1 only, the last 0.58 Myrs) range from <20 m along the Florida panhandle, to ~65 m along the Texas coast, to upwards of ~125 m in the Mississippi Delta region.

Dip-oriented profiles display the expected increasingly thick wedge of sediment moving in the basinward direction (Figure 5a–d), from the coastal plain to the shelf margin, a pattern recognised in the classic early work of Fisk and McFarlan (1955). For the Mississippi depocentre at −90.88°W (Figure 5b), Plio-Pleistocene thicknesses increase from ~220 m at the latitude of Baton Rouge, Louisiana (30.5°N), to ~1,700 m at the modern deltaic shoreline (~29°N), and >3,000 m at the shelf margin (~28°N). These thicknesses are in general agreement with earlier published findings (Blum & Roberts, 2012; McFarlan & LeRoy, 1988; Woodbury et al., 1973). By

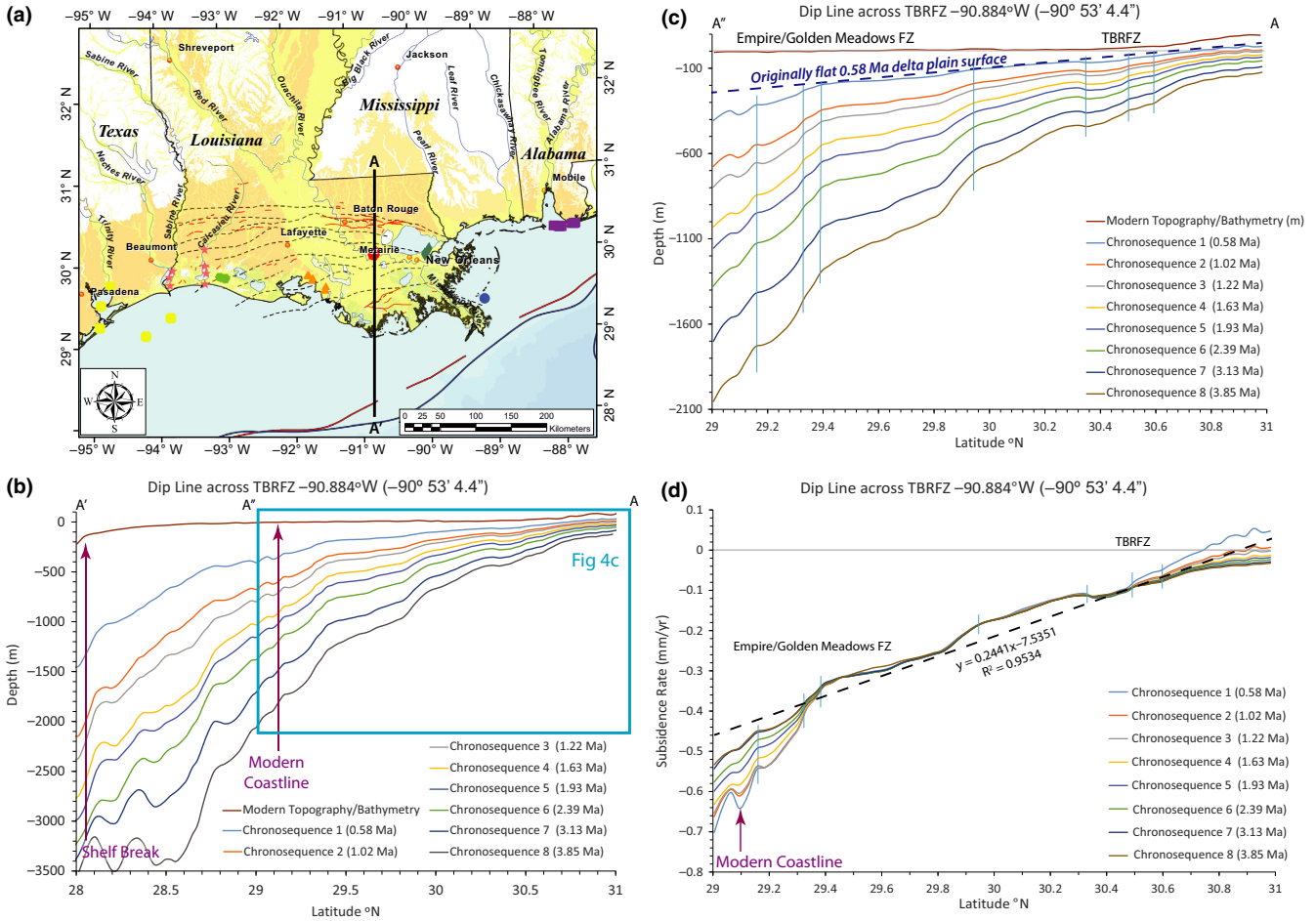

FIGURE 5 Dip-oriented cross sections of Plio-Pleistocene chronosequence tops across the Lower Mississippi River alluvial valley to the coastline and shelf margin. Present day latitude location of coastline, shelf break, Empire/Golden Meadows and Tepetate-Baton Rouge Fault Zones identified (Murray, 1961). A = Generalised geologic location map with dip line section shown in plan view. Pleistocene alluvial-deltaic deposits shown in orange; Holocene deposits shown in yellow. Sites where published Holocene sea level records have been defined shown by coloured symbols, as indicated in Figure 1 legend. B = Dip line cross section through Middle Pleistocene to Late Pliocene chronostratigraphic surfaces extending to the shelf break. C = Dip line cross section through Middle Pleistocene to Late Pliocene chronostratigraphic surfaces extending to the delta front coastline. Dashed line highlights vertical displacement deviations from the original 0.58 Ma delta plain surface as a result of fault motion, salt movement, and isostatic loading. D = Dip line subsidence rate cross section through Middle Pleistocene to Late Pliocene chronostratigraphic surfaces extending to the delta front coastal zone

TABLE 2 Calculated fault throw rates along dip line sections at the intersection of fault planes and Chronosequence 1, 3, & 7 boundaries (McCulloh & Heinrich, 2013; Murray, 1961)

Longitude (°)	Latitude (°)	Seq 1 fault throw (m)	Seq 1 time-averaged throw rate (mm/year)	Seq 3 fault throw (m)	Seq 3 time-averaged throw rate (mm/year)	Seq7 fault throw (m)	Seq 7 time-averaged throw rate (mm/year)
92.5	30.55	11.55	0.0199	16.41	0.0135	32.92	0.0105
92	30.55	4.98	0.0086	9.59	0.0079	23.38	0.0075
91.5	29.7	10.36	0.0179	6.40	0.0052	63.09	0.0202
91.5	29.95	10.05	0.0173	21.03	0.0172	76.2	0.0243
91.5	30.5	3.04	0.0052	6.51	0.0053	18.29	0.0058
91	29.8	10.67	0.0184	21.19	0.0174	76.2	0.0243
91	30.05	10.36	0.0179	20.08	0.0165	49.07	0.0157
91	30.35	6.73	0.0116	3.26	0.0027	38.71	0.0124
90.5	30.5	12.43	0.0214	19.58	0.0160	50.15	0.0160
90	29.7	6.71	0.0116	13.19	0.0108	53.04	0.0169
90	30.45	9.85	0.0170	13.69	0.0112	43.46	0.0139
	Average	8.80	0.0152	13.72	0.0112	47.68	0.0152

Due to oblique nature of longitudinal dip line extraction relative to the true dip of the fault, the above-referenced throw estimates and rates are conservative. Consistent with Shen et al. (2017) fault throw was measured as the vertical offset of facies boundaries originally horizontal. Dividing the throw by the chronostratigraphic time interval produces a time-averaged throw rate.

comparison, corresponding thicknesses for the middle Pleistocene to present range from ~45 m at 30.5°N, to ~400 m at the modern deltaic shoreline (~29°N), and >1,400 m at the shelf margin (~28°N). These dip-oriented profiles also show locations and offsets associated with seaward-dipping normal faults and associated rollover structures (Figure 5c), including the Tepetate-Baton Rouge fault zone (TBRFZ) (McCulloh & Heinrich, 2013), as well as additional regional growth faults that have been mapped laterally and downdip across south Louisiana (Murray, 1961). Fault displacements are discussed below.

4.2 | Subsidence rates

Strike-oriented cross sections extracted along the northern GOM coastline and through specified Holocene sea-level study sites illustrate the alongshore range of deep-seated subsidence values (see Figures 4,6). When measured from the base of Chronosequence 7, ca. 3.1 Ma, time-averaged deep-seated subsidence rates in the broader Mississippi depocentre (−90 to −93°W) are ~0.22 mm/year, whereas rates are <0.12 mm/year along the east Texas coast, and <0.02 mm/year in Alabama and the Florida panhandle. This order of magnitude spatial variability in rates across the northern GOM coast, and associated absolute magnitudes, are not significantly different when using the base of Chronosequence 1 at ca. 0.58 Ma instead. Moreover, these rates are consistent with, but slightly higher than, Middle Miocene to present time-averaged subsidence rates of 0.13 mm/year calculated by Edrington et al. (2008) in the Michoud area of East New Orleans, and consistent with the low rates measured by Straub et al. (2009) some 100 km farther south in Black Bay, Louisiana.

As expected, dip-oriented profiles display increasing rates of subsidence from north to south, from the coastal plain to the shelf margin. Figure 5d highlights an average linear regression fit slope of 0.2441 mm/year for the Late Pliocene (3.85 Ma) with an R^2 of >0.95. These deep-seated subsidence estimates are an order of magnitude lower than previously published deep-seated subsidence linear regression estimates derived from GPS data for the Lower Mississippi Delta region (Jankowski et al., 2017; Karegar et al., 2015).

FIGURE 6 Plot of time-averaged subsidence along the Gulf of Mexico coastline, extracted from gridded chronosequence datasets for the late Pliocene and mid Pleistocene from southern Alabama across the Mississippi depocenter to east-central Texas, as compared with fault and sea level measurement sample locations. Fault symbols (–▪–) represent locations where the data extraction line crosses regional growth faults as mapped in Murray (1961). Letters represent sea-level data sampling locations: A = Rodriguez et al. (2004, 2005), B = Milliken et al. (2008), C = Yu et al. (2012), D = Törnqvist et al. (2006), E = Törnqvist et al. (2004), F = Edrington et al. (2008), and G = Blum et al. (2003). Note: Onshore depths and calculated subsidence rates at incised valley locations (e.g. ~−91.8 and ~−86.75°W) may be subject to down-stacking and Plio-Pleistocene data scarcity bias

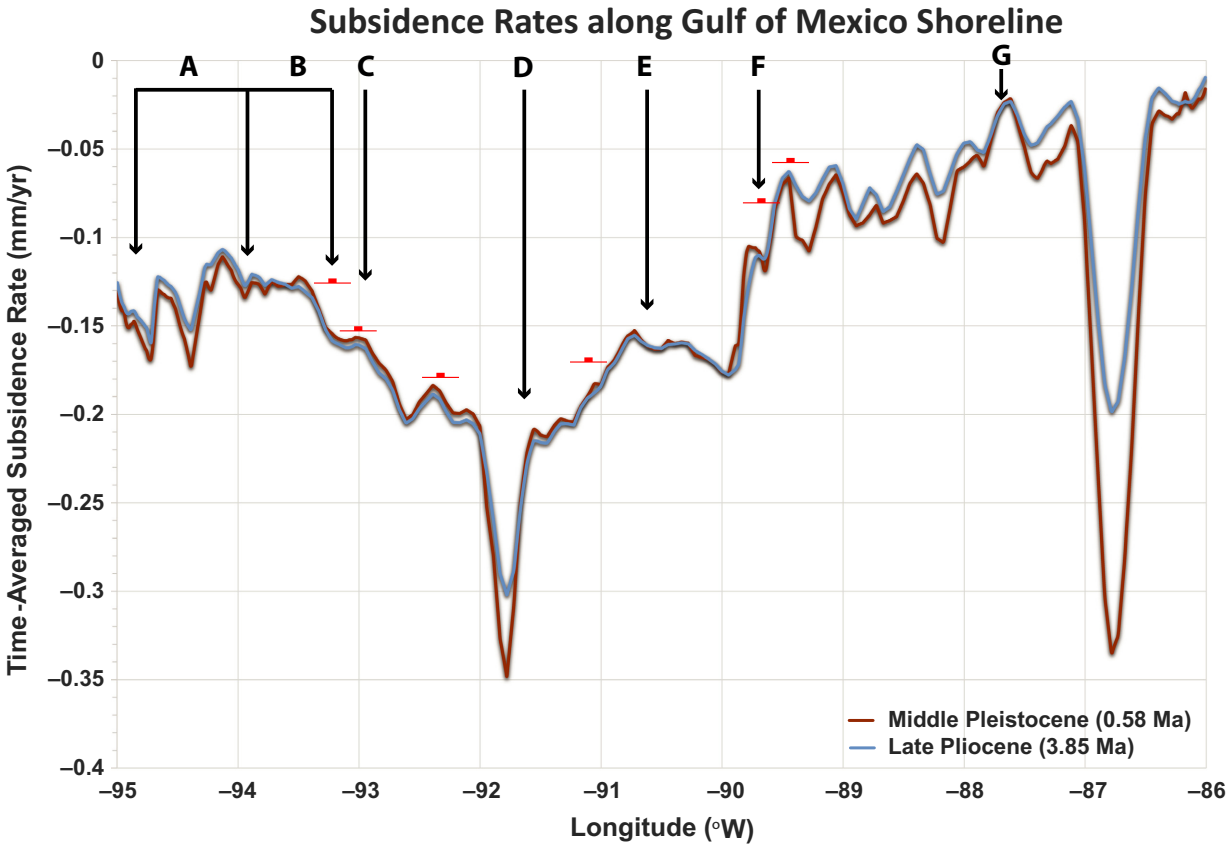
Subsidence Rates along Gulf of Mexico Shoreline
A
B
C
D
E
F
G
0
−0.05
−0.1
−0.15
−0.2
−0.25
−0.3
−0.35
−0.4
Time-Averaged Subsidence Rate (mm/yr)
−95
−94
−93
−92
−91
−90
−89
−88
−87
−86
Longitude (°W)
Middle Pleistocene (0.58 Ma)
Late Pliocene (3.85 Ma)

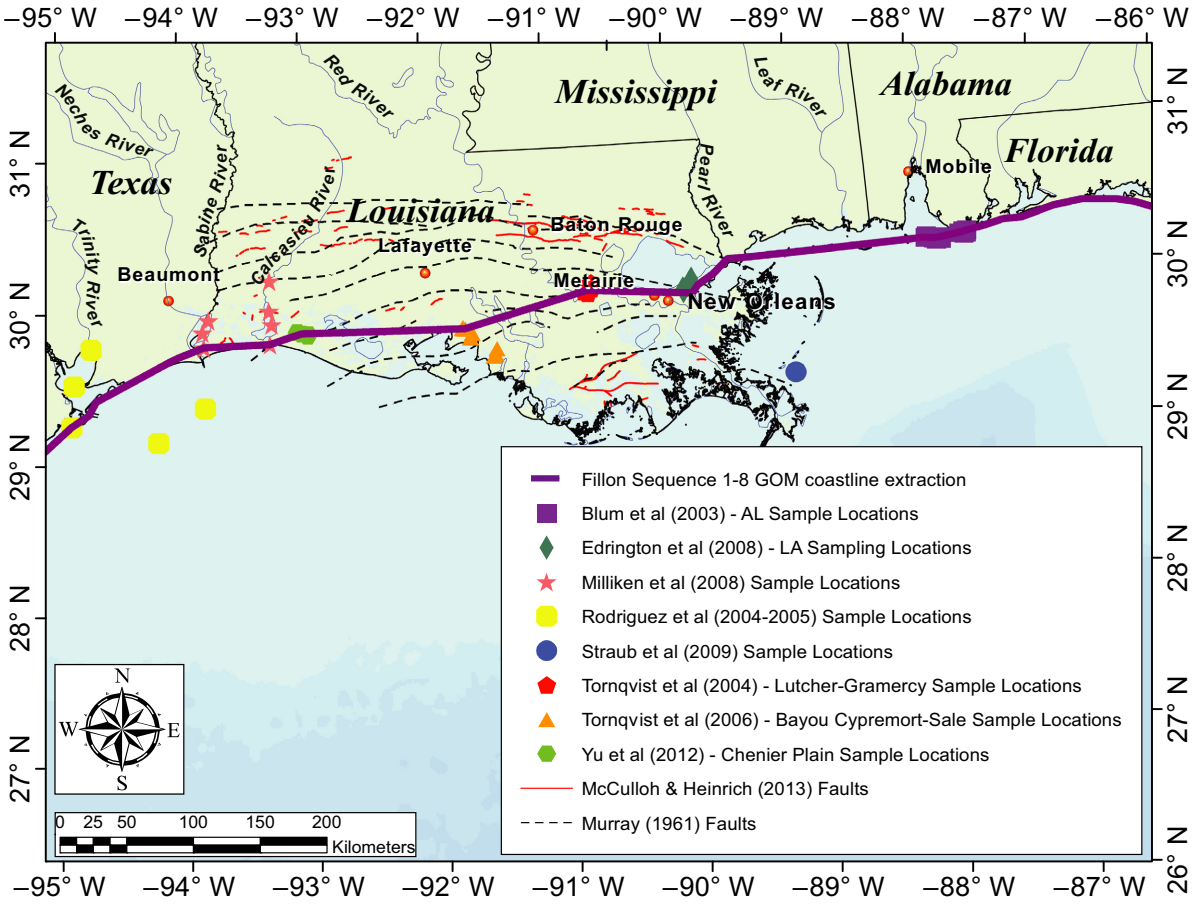
−95° W
−94° W
−93° W
−92° W
−91° W
−90° W
−89° W
−88° W
−87° W
−86° W
31° N
30° N
29° N
28° N
27° N
26° N
Mississippi
Alabama
Florida
Texas
Louisiana
Red River
Neches River
Sabine River
Calcasieu River
Trinity River
Leaf River
Pearl River
Mobile
Baton Rouge
Lafayette
Beaumont
Metairie
New Orleans
Fillon Sequence 1-8 GOM coastline extraction
Blum et al (2003) - AL Sample Locations
Edrington et al (2008) - LA Sampling Locations
Milliken et al (2008) Sample Locations
Rodriguez et al (2004-2005) Sample Locations
Straub et al (2009) Sample Locations
Tornqvist et al (2004) - Lutcher-Gramercy Sample Locations
Tornqvist et al (2006) - Bayou Cypremort-Sale Sample Locations
Yu et al (2012) - Chenier Plain Sample Locations
McCulloh & Heinrich (2013) Faults
Murray (1961) Faults
N
W
E
S
0 25 50 100 150 200
Kilometers

TABLE 3 Calculated percentage of throw rate relative to deep-seated subsidence rate along dip line sections at the intersection of fault planes and Chronosequence 1, 3, & 7 boundaries (McCulloh & Heinrich, 2013; Murray, 1961)

Longitude (°)	Latitude (°)	Seq1 subsidence Rate (mm/year)	Seq 1 fault throw percent of subsidence rate (%)	Seq 3 subsidence rate (mm/year)	Seq 3 fault throw percent of subsidence rate (%)	Seq 7 subsidence rate (mm/year)	Seq 7 fault throw percent of subsidence rate (%)
92.5	30.55	0.0496	40.12	0.0637	21.19	0.0714	14.70
92	30.55	0.0689	12.48	0.0747	10.57	0.0779	9.63
91.5	29.7	0.2779	6.44	0.2791	1.86	0.2793	7.23
91.5	29.95	0.2142	8.08	0.2158	7.97	0.2149	11.31
91.5	30.5	0.0846	6.15	0.0898	5.90	0.0926	6.26
91	29.8	0.2542	7.24	0.2579	6.75	0.2594	9.36
91	30.05	0.1744	10.24	0.1763	9.36	0.1775	8.85
91	30.35	0.1167	9.94	0.1195	2.26	0.1217	10.19
90.5	30.5	0.0911	23.49	0.0969	16.51	0.1020	15.69
90	29.7	0.2548	4.55	0.2552	4.23	0.2554	6.62
90	30.45	0.0926	18.35	0.0967	11.58	0.0977	14.23
	Average	0.1526	13.37	0.1569	8.953	0.1591	10.37

Due to oblique nature of longitudinal dip line extraction relative to the true dip of the fault, the above-referenced throw estimates and rates are conservative. Consistent with Shen et al. (2017) fault throw was measured as the vertical offset of facies boundaries originally horizontal. Dividing the throw by the chronostratigraphic time interval produces a time-averaged throw rate.

When calculated separately, subsidence rates for all Plio-Pleistocene sequences converge to zero at ~30.75°N, with modest uplift projected to the north. For the middle to late Pleistocene (the last 0.58 Myrs), subsidence rates are ~0.7 mm/year at the present-day deltaic shoreline, and ~2.4 mm/year at the shelf margin. However, between 30.5 and 28.5°N, rates decrease slightly through time, such that older chronostratigraphic sequences show slightly higher rates, whereas farther basinward, rates increase through time, and younger chronostratigraphic sequences show higher rates. This trend likely reflects progradation of the margin with a modest basinward shift of loads, and is increasingly apparent in older and more deeply buried Neogene sequences, which have inland equivalents that have been flexurally uplifted (e.g., Shen et al., 2012; Wolstencroft et al., 2014).

Dip-oriented profiles also permit calculations of the cumulative throw and time-averaged throw rate on growth fault planes within the Mississippi Delta plain through the Plio-Pleistocene (Table 2), so as to isolate the contributions of faults to deep-seated subsidence (Figure 5c). Calculations for fault throw are inherently distinct from fault offset measurements in that by definition the horizontal component of motion is excluded (Spurr, 1897). Calculation of mean fault throw rates assume that the upper bounded surface was originally horizontal and that the sedimentary unit was deposited at timescales significantly shorter than those over which the throw rate is calculated. Common for the well-known TBRFZ and other normal growth faults in the Lower Mississippi Delta region, cumulative throw rates increase with depth, whereas individual time-averaged throw rates generally decrease with depth or stay near constant.

In the eastern part of the Mississippi depocentre, at −90.5°W, movement within the TBRFZ occurred at a rate of 0.0214 mm/year during deposition of Chronosequence 1 (0.58 Ma to present), and at 0.016 mm/year during deposition of Chronosequence 7 (3.1–2.4 Ma). By contrast, the western boundary of the TBRFZ at −91.5°W shows laterally variability in throw with substantially lower mean throw rates of 0.0052 mm/year in Chronosequence 1 and 0.0058 mm/year in Chronosequence 7 (Table 2). Generally, throw rates are lower for Chronosequence 1, 3 & 7 than the time-averaged rates reported in Shen et al. (2017) for the Holocene, but consistent with their rates averaged over the last interglacial period to present. Fault throw rates trends decline or remain relatively constant in successively deeper chronosequence units resulting in substantial variability (e.g., ~4.5%–40%) relative to generally consistent total deep-seated subsidence rates (Table 3).

Farther downdip, on the southern margins of the subaerial delta plain (29.4–29°N), a series of growth faults have long been recognised (e.g., Murray, 1961): these include the Empire, Golden Meadow and other faults (e.g., Armstrong, Mohrig, Hess, George, & Straub, 2014; Chan & Zoback, 2007; Gagliano, Kemp, Wicker, Wiltenmuth, & Sabate, 2008; Kuecher, Roberts, Thompson, & Matthews, 2001; Roberts, Morton, & Freeman, 2008), which show

evidence for surface or near-surface rupture. Gagliano et al. (2008) and others argue that movement along such growth faults is a major contributor to land-surface subsidence and coastal wetland loss. From our data, actual rates of fault movement are difficult to disentangle for older chronosequences, but cumulative throw across this zone for Chronosequence 1 is 6.71 m, which defines a maximum time-averaged rate of 0.012 mm/year (Table 2), and here again accounts for only ~4.5% of the total deep-seated subsidence for the 0.58 Ma surface (Table 3) at the present-day shoreline (~29°N).

5 | DISCUSSION

Plio-Pleistocene chronostratigraphic data provide the first quantitative estimates for regional rates of deep-seated subsidence and their spatial variability for the Mississippi depocentre and adjacent parts of the GOM shoreline. Within the area of the present Mississippi Delta plain, where subsidence and land loss is an existential crisis, deep-seated subsidence rates approach ~0 mm/year between 31 and 30.5°N, then increase to ~0.7 mm/year at ~29°N, which approximates the present deltaic shoreline. This deep-seated subsidence component accounts for <10% of the total land-surface subsidence measured by Jankowski et al. (2017), and most land-surface subsidence therefore likely represents compaction and dewatering of the thick, shallow Holocene fluvial-deltaic succession (e.g. Blum & Roberts, 2012; Törnqvist et al., 2008). Our analyses also estimate the time-averaged contributions of growth faults to the deep-seated subsidence component. In both updip and downdip locations, time-averaged throw rates indicate that growth faults that impact the 0.58 Ma chronostratigraphic surface account for no more than ~40% of the total deep-seated subsidence for faulted parts of that surface. For updip locations, specifically the TBRFZ, our results show a decrease in throw rates when they are measured in older chronostratigraphic sequences. Our results for the last 0.58 Ma are consistent with estimates by Shen et al. (2017) for the updip TBRFZ over the last glacial-interglacial cycle (timescale of ~0.13 Ma), but lower than values they obtained when they isolate throw rates for the relatively short late Holocene (~0.003 Ma).

We also note along-strike variability in throw rates, which may reflect interactions between different growth faults (Cowie & Roberts, 2001). Lateral variations in fault motion across the TBRFZ appear directly dependent upon Holocene stratal thickness (Roberts et al., 1994), similar to the linear relationship between overburden thickness and compaction rates of up to 5 mm/year noted by Törnqvist et al. (2008). Although some authors have proposed deep basal fault motion with potential buttressing stress constraint associated with downdip sediment and allochthonous salt movement/structure in southeast Louisiana (Dokka et al., 2006; McBride, Rowan, & Weimer, 1998; Shen et al., 2017), additional investigation of lateral and vertical slip rates across regional faults through Quaternary stratigraphy would be required to demonstrate fault interaction due to the inherent regional biostratigraphic sampling sparsity and uncertainties translated with depth. Other authors continue to propose much more significant aseismic growth faulting contributions to the deep-seated subsidence impacting the Southeastern Louisiana delta plain (Gagliano et al., 2008; Stephens, 2010). Taken at face value, the quantifiable displacement along the Empire-Golden Meadows fault zone (Gagliano, 2003) supported by Grand Isle tide gauge measurements (Morton & Bernier, 2010) represents significant acceleration and deceleration of localised subsidence associated with intermittent fault motion over a period of less than two decades (Blum & Roberts, 2012). By comparison, these reported intermittent annualised subsidence rates of 10–15 cm/year would represent over 1,800 years of deep-seated subsidence motion. Our deep-seated subsidence data and analyses of vertical fault motion from 0.58 to 3.85 Ma highlights the limited contribution of growth faulting across geologic timescales and further reinforces the significant contribution of Holocene sediment compaction and dewatering in measured geodetic rates of subsidence.

From these chronostratigraphic data, time-averaged deep-seated subsidence rates are shown to increase as the length of time-averaging decreases (Figure 7), an example of the inverse relationship between rates of geologic processes and the timescale of measurement similar to those first identified by Sadler (1981, 1999); (see also Meckel, 2008; Schumer & Jerolmack, 2009). This inverse relationship becomes more pronounced when compared to historical published GOM subsidence rate measurements from geodetic data over decadal timescales, or basal peat ^{14}C data from the Pleistocene-Holocene stratal contact representing century to millennial timescales. Rod surface elevation table marker horizon and geodetically derived shallow-seated or total subsidence rates can be more than two orders of magnitude higher than either deep-seated subsidence rates, or time-averaged rates throw rates of growth faults. For stratigraphic measurements, this inverse relationship is due to the increased prevalence of hiatuses in section as the timescale for measurement increases. Across the Mississippi Delta subsidence, however, this inverse relationship reflects the contributions of different processes to the actual measurement over time, as follows: (a) over years to decades, short-term transient phenomena, for example a period of rapid movement along a growth fault, can dominate the measured signal of land-surface subsidence (Dokka et al., 2006; Shinkle & Dokka, 2004); (b)

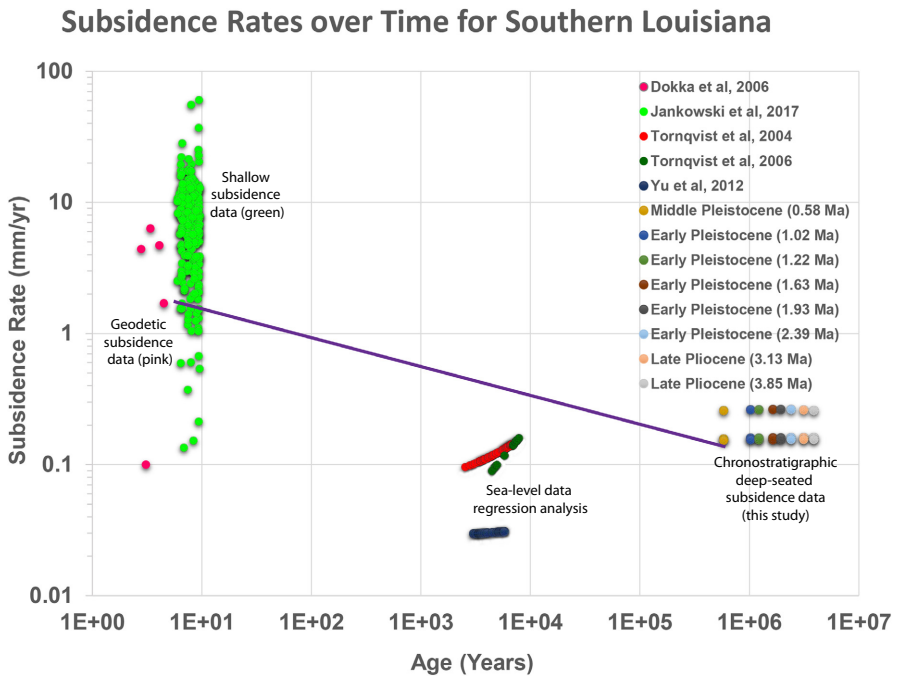

FIGURE 7 A compilation of subsidence rates versus time as derived from different datasets. Subsidence rates plotted based upon historic regional scientific research as extracted from Lower Mississippi River basin chronostratigraphic data. This figure highlights the significant inverse relationship between rates of geologic processes and the timescale of measurement, similar to those first identified by Sadler (1981). Geodetic, shallow, and deep-seated subsidence datasets are each dominated by disparate geological processes. Subsidence rate derivation from basal peat geochronology data followed second-order polynomial regression analysis methodologies as described by Törnqvist et al. (2006) and Yu et al. (2012). These regression analysis methodologies incorporated 2σ uncertainities in the vertical (elevation) and horizontal (age) directions of sea level index points by polynomial curve fitting. Resultant differences between upper and lower regression surfaces have been historically advanced as a very conservative representation of flexural lithospheric subsidence rates due to sediment loading and glacial isostatic effects

over annual to millennial-scale time periods, compaction and dewatering of recently deposited sediments dominate the signal; and (c) over 10^4–10^5 years with thick stratigraphic sections, depocentre-scale isostatic and fault-related processes dominate the signal (Watts, Zhong, & Hunter, 2013). We concur with Blum and Roberts (2012), Shen et al. (2017), Nienhuis, Törnqvist, Jankowski, Fernandes, and Keogh (2017), and Jankowski et al. (2017) that, over the century-scale time period of relevance to Mississippi Delta survival, land-surface subsidence is dominated by shallow-seated processes (sediment compaction and dewatering) and that deep-seated processes (such as growth fault motion) generally play a secondary role.

Our data also bears on published interpretations of Holocene sea-level change. On one end of the spectrum, previous workers have argued that the Holocene-Pleistocene contact in the Mississippi Delta region is tectonically stable (<0.25 mm/year) attributable to gradual seaward shifts in the principal clastic depocentre. Basal peats from the Holocene-Pleistocene contact would thereby define a representative GOM sea-level curve (Törnqvist et al., 2006). Sea-level reconstructions from the Texas coast (e.g., Milliken et al., 2008; Simms et al., 2007) similar in pattern and rate of change to those from basal peats in the delta region, have likewise been argued to represent a regionally applicable GOM record. On the other end of the spectrum, a number of workers (e.g., Blum et al., 2001, 2003; Morton et al., 2000) have interpreted Holocene coastal landforms to indicate that sea-level outside of the subsiding delta region reached present elevations by the middle Holocene, ca. 6 Ka, and has been close to present since that time. Blum et al. (2008) suggested any resemblances in sea-level curves between areas within and outside of the deltaic depocentre could be no more than a coincidental convergence of results from different processes.

We have measured the deep-seated subsidence component along the present-day GOM coastline, from the Florida panhandle, across the deltaic depocentre, and to east Texas, through the locations where published studies of Holocene sea-level change have been conducted. Deep-seated subsidence rates measured from the base of Chronosequence 1 (ca. 0.58 Ma) are 0.025 mm/year in Gulf Shores, Alabama (studies by Blum et al., 2001, 2003; Rodriguez & Meyer, 2006), 0.22 mm/year within the present Mississippi valley (studies by Törnqvist et al., 2004, 2006), 0.161 mm/year on the Chenier Plain of Louisiana (studies by Milliken et al., 2008; Yu et al., 2012), and 0.150 mm/year in Galveston, TX (studies by Milliken et

al., 2008). Deep-seated subsidence rates within the Mississippi depocentre are therefore an order of magnitude greater than they are at sites where Holocene sea-level change has been examined in Florida and Alabama, and 50% greater than they are in west Louisiana and east Texas, when they are averaged over the last 0.58 Ma. The deep-seated subsidence component we have measured here is not of sufficient magnitude to reconcile differences between sea-level curves, but is sufficient to note that sea-level curves from the delta region cannot be representative of the GOM as a whole.

Finally, we consider our measured deep-seated rates to be minimum values that would increase if we were able to measure shorter and younger time intervals, and shorter and younger time periods would be dominated by slightly different processes as well. For example, Galloway, Ganey-Curry, and Whiteaker (2009) has defined 18 GOM Cenozoic transgressive depositional episodes (deposodes) that identify changes in ice, ocean and sediment loading at the continental shelf and margin over timescales of thousands of years. In addition, Blum et al. (2008) modelled isostatic response to valley cutting and filling during the last glacial cycle, and identified a cyclical pattern of isostatic adjustments over latest Pleistocene and Holocene timescales: uplift results from valley cutting and removal of strata during the glacial period, and subsidence results from valley filling during post-glacial sea-level rise. The Blum et al. (2008) modelled shoreline flexure is consistent with the present elevations of middle to late Holocene sea-level indicators in the delta region and farther east near Gulf Shores, Alabama. However, Wolstencroft et al. (2014) show that their model used elastic thickness values that were too low, which exaggerated the overall amplitude of uplift and subsidence. Regardless, isostatic responses to changes in ice and sedimentation load over 10^3–10^5 years (Miller et al., 2005, 2011; Pitman & Golovchenko, 1983) must produce a short to moderate-term subsidence component that is embedded within the cumulative longer term subsidence we have measured, that must then be accounted for in studies of Holocene sea-level change. Yu et al. (2012) attempted to quantify this lithospheric flexure subsidence in the Chenier Plain, on the western bounds of the Mississippi Delta incised valley, through a very conservative 2σ regression curve difference methodology (Figure 7). Although their results revealed a 0.15 ± 0.7 mm/year differential rate of subsidence between the Chenier Plain and portions of the Mississippi Delta, our results herein suggest a more dynamic deep-seated subsidence record extending to the west given the varied geologic history of Texas Gulf Coast fluvial system input (Galloway, Whiteaker, & Ganey-Curry, 2011). Love, Milne, Tarasov, Engelhart, and Hijma (2016) recently modelled the glacial isostatic adjustment (GIA) contribution to sea-level change, including ice and ocean isostatics, in the Mississippi Delta region with adjustments of up to ~0.35 mm/year. However, spatial and temporal dynamic sedimentation contributions resulting from glacial-interglacial fluvial discharge and drainage basin reorganisation in the mixed bedrock alluvial valley system remain largely unconstrained along this broad, depositional coastline, which raises the question of whether there can be a representative sea-level curve.

6 | CONCLUSION

Our findings represent the first regional-scale quantitative study of deep-seated subsidence rates for the northern Gulf of Mexico, including the Mississippi depocentre, and provide a regional baseline for lithospheric response to loading beneath one of the world's largest deltas. Our detailed examination of Middle Pleistocene (0.58 Ma) to the Late Pliocene (3.85 Ma) gridded chronostratigraphic surfaces derived from 80,928 well reports from across the GOM illustrates the temporal and spatial patterns of sediment thickness and the magnitude of subsidence processes across northern GOM. Quantification of deep-seated subsidence rate components and spatial variability, extending from geologically long-time to short-time frames, are not only central to understanding coastal land loss in the Mississippi Delta region, but also contribute to different scientific hypotheses of the northern GOM RSL record. We show that, when viewed along-strike parallel to the coastline, time-averaged deep-seated subsidence rates over the last 0.58 Myrs are ~0.16–0.22 mm/year in the Mississippi depocentre (−90 to −93°W), versus <0.12 mm/year along the east Texas coast, and <0.02 mm/year in Alabama and the Florida panhandle. When measured in the dip direction for the middle to late Pleistocene (the last 0.58 Myrs), subsidence rates within the Mississippi depocentre approach zero at ~30.5°N, with modest uplift projected to the north, and increases in rates to the south, with ~0.7 mm/year at the present-day deltaic shoreline, and ~2.4 mm/year at the shelf margin.

The time-averaged deep-seated subsidence component over the last 0.58 Myrs accounts for <10% of the total land-surface subsidence as measured (~10 mm/year) over decadal timescales from 274 sites along the Louisiana coastline (Jankowski et al., 2017). This observation highlights the time-dependence of different process contributions to the total subsidence signal. The direct, inverse logarithmic relationship between subsidence rate measurements and duration of the time period of measurement is indicative of how different subsidence processes dominate the measured signal over different timescales: (a) across annual timescales, dewatering and primary sediment consolidation processes dominate; (b) from years to decades,

short-term, transient processes dominate such as growth fault movement; (c) over century to millennial timescales, sediment loading and compaction is the most important process; and (d) over timescales of 10^4–10^5 years, the accumulation of thick fluvial-deltaic strata and corresponding depocentre scale isostatic processes (e.g., lithospheric flexure, faulting, and allochthonous salt movement) dominate the measured subsidence signal.

The contribution of growth fault movement to total land-surface subsidence, beyond the decadal timescale, appears to be very small: in both the updip and downdip directions, rates of vertical fault displacement accounted for ~4.5%–40% of the total subsidence over the last 0.58 Myrs, with decreasing throw rates in successively deeper units. Moreover, there is some along-strike variability in throw rates, directly correlating to Holocene stratal thickness (Roberts et al., 1994) and potential growth fault interaction at depth (Cowie & Roberts, 2001). Progressively deeper strata are influenced by different deep-seated subsidence components with ever older and longer time frames trending to the minimum measured deep-seated rates presented here. In aggregate these findings reinforce the view that the vast majority (~80%) of geodetically recorded total land-surface subsidence rates measured during the historic period represent compaction and dewatering of the thick, shallow Holocene fluvial-deltaic succession (e.g., Blum & Roberts, 2012; Meckel et al., 2006; Törnqvist et al., 2008).

Finally, quantification of deep-seated subsidence rates and their spatial variability provide insight into the complexities of interpretations of the Holocene record of relative sea-level change. The northern GOM coastline, with its accumulation of spatially variable fluvial-deltaic loads over time caused by fluvial drainage basin reorganisations, must have a spatially variable long-term isostatic response as described herein. Moreover, across Milankovich cycles of thousands of years, when river cut valleys during sea-level fall, and fill them during sea-level rise, isostatic responses to changes in load produce a short-term cycle of uplift and subsidence that is superimposed on the cumulative longer term deep-seated subsidence rates presented here (Blum et al., 2008; see also Ivins, Dokka, & Blom, 2007; Syvitski, 2008). The sum total of isostatic rates are likely not sufficient to fully reconcile differences between sea-level curves measured along the northern GOM coastline, but they do confirm that sea-level curves derived from the delta region cannot be representative of the GOM as a whole.

With quantified coastal land loss also documented at the Nile, Yellow, Indus, Ebro, and Rhone delta regions due to a combination of engineered and environmental (e.g., eustasy and subsidence) RSL impacts (Syvitski, 2008), and current global mean sea-level rates rising at rates three times faster than during Holocene Mississippi Delta plain construction (Blum & Roberts, 2012), the associated lives and wetland habitats are under increasing threat to storm surge and salt water inundation globally. Our findings constitute the primary study of Plio-Pleistocene deep-seated subsidence records and chronostratigraphic surfaces, providing a regional baseline for lithospheric isostatic response extending beneath one of the world's largest deltas, providing both constraint for climate change impact models and potential motivation for additional subsidence investigations across global, threatened fluvial-deltaic depocentres currently providing sustenance and shelter to millions.

ACKNOWLEDGEMENTS

Support for this work was provided by the Ritchie Distinguished Professorship in the Department of Geology, University of Kansas. We also would like to thank Drs. Torbjorn Tornqvist, Kyle Straub, and one anonymous reviewer for their commentary and editorial efforts to improve this manuscript.

REFERENCES

Armstrong, C., Mohrig, D., Hess, T., George, T., & Straub, K. M. (2014). Influence of growth faults on coastal fluvial systems: Examples from the Late Miocene to Recent Mississippi River Delta. *Sedimentary Geology*, *301*, 120–132. https://doi.org/10.1016/j.sedgeo.2013.06.010

Batker, D., Mack, S., Skylar, F., Kelly, M., Freeman, A., Nuttle, W., & Costanza, R. (2012) What Louisiana stands to lose. 28–31.

Blum, M. D., Carter, A. E., Zayac, T., & Goble, R. (2002). Middle Holocene sea-level and evolution of The Gulf of Mexico Coast (USA). *Journal of Coastal Research*, *36*, 65–80. https://doi.org/10.2112/1551-5036-36.sp1.65

Blum, M. D., Misner, T. J., Collins, E. S., Scott, D. B., Morton, R. A., & Aslan, A. (2001). Middle Holocene sea-level rise and highstand at +2 m, Central Texas Coast. *Journal of Sedimentary Research*, *71*, 581–588. https://doi.org/10.1306/112100710581

Blum, M. D., & Roberts, H. H. (2009). Drowning of the Mississippi Delta due to insufficient sediment supply and global sea-level rise. *Nature Geoscience*, *2*, 488–491. https://doi.org/10.1038/ngeo553

Blum, M. D., & Roberts, H. H. (2012). The Mississippi Delta region: past, present, and future. *Annual Review of Earth and Planetary Sciences*, *40*, 655–683. https://doi.org/10.1146/annurev-earth-042711-105248

Blum, M. D., Sivers, A. E., Zayac, T., & Goble, R. J. (2003). Middle Holocene sea-level and evolution of the Gulf of Mexico coast. *Gulf Coast Association of Geological Societies Transactions*, *53*, 64–77.

Blum, M. D., Tomkin, J. H., Purcell, A., & Lancaster, R. R. (2008). Ups and downs of the Mississippi Delta. *Geology*, *36*, 675–678. https://doi.org/10.1130/G24728A.1

Cazenave, A., Dieng, H.-B., Meyssignac, B., von Schuckmann, K., Decharme, B., & Berthier, E. (2014). The rate of sea-level rise. *Nature Climate Change*, *4*, 358–361. https://doi.org/10.1038/nclimate2159

Cazenave, A., & Llovel, W. (2010). Contemporary sea level rise. *Annual Review of Marine Science*, *2*, 145–173. https://doi.org/10.1146/annurev-marine-120308-081105

Chan, A. W., & Zoback, M. D. (2007). The role of hydrocarbon production on land subsidence and fault reactivation in the Louisiana Coastal Zone. *Journal of Coastal Research*, *23*, 771–786. https://doi.org/10.2112/05-0553

Church, J. A., Clark, P. U., Cazenave, A., Gregory, J. M., Jevrejeva, S., Levermann, A., … Unnikrishnan, A. S. (2013) Sea level change, *in* Climate Change 2013: The Physical Science Basis. Contribution of Working Group I to the Fifth Assessment Report of the Intergovernmental Panel on Climate Change. 1137–1216. https://doi.org/10.1017/cb09781107415315.026

Cowie, P. A., & Roberts, G. P. (2001). Constraining slip rates and spacings for active normal faults. *Journal of Structural Geology*, *23*, 1901–1915. https://doi.org/10.1016/S0191-8141(01)00036-0

Diegel, F. A., Karlo, J. F., Schuster, D. C., Shoup, R. C., & Tauvers, P. R. (1995). Cenozoic structural evolution and tectono-stratigraphic framework of the Northern Gulf Coast Continental Margin: Salt tectonics: A global perspective: AAPG Memoir 65, 109–151.

Dixon, T. H., Amelung, F., Ferretti, A., Novali, F., Rocca, F., Dokka, R., … Whitman, D. (2006). Space geodesy: Subsidence and flooding in New Orleans. *Nature*, *441*, 587–588. https://doi.org/10.1038/441587a

Dokka, R. K. (2011). The role of deep processes in late 20th century subsidence of New Orleans and coastal areas of southern Louisiana and Mississippi. *Journal of Geophysical Research*: Solid: Earth, *116*, 1–25. https://doi.org/10.1029/2010JB008008

Dokka, R. K., Sella, G. F., & Dixon, T. H. (2006). Tectonic control of subsidence and southward displacement of southeast Louisiana with respect to stable North America. *Geophysical Research Letters*, *33*, 1–5. https://doi.org/10.1029/2006GL027250

Donnelly, J. P., & Giosan, L. (2008). Tempestuous highs and lows in the Gulf of Mexico. *Geology*, *36*, 751–752. https://doi.org/10.1130/focus092008.1

Edrington, C. H., Blum, M. D., Nunn, J. A., & Hanor, J. S. (2008). Long-term subsidence and compaction rates: A new model for the Michoud area, south Louisiana: Transactions - Gulf Coast Association of Geological Societies. *58*, 261–272.

Fillon, R. H. (2007). Wilcox Depositional Architecture in the Gulf of Mexico Basin: A framework for improving deep water exploration and reservoir risk, *in* 27th Annual GCSSEPM Foundation Bob F. Perkins Research Conference. 79–100.

Fillon, R. H. (2016). Chronostratigraphic views of Gulf of Mexico tectonic and deposystem evolution in the mesozoic. In GCSSEPM 35th Annual Bob F. Perkins and Norm C. Rosen Research Conference "Mesozoic of the Gulf Rim and Beyond: New Progress in Science and Exploration of the Gulf of Mexico Basin" (p. 43). Houston, TX.

Fisk, H. N., & McFarlan Jr., E. (1955). Late quaternary deltaic deposits of the Mississippi River. In A. Poldervaart (Ed.), *Crust of the earth*. Special Papers Geological Society of America, (vol. 62, pp. 279–302).

Gagliano, S. M. (2003). Active geological faults and land change in Southeastern Louisiana.

Gagliano, S. M., Kemp, E. B. III, Wicker, K. M., Wiltenmuth, S., & Sabate, R. W. (2008). Neo-tectonic framework of SE Louisiana and applications to Coastal Restoration: GCAGS Transactions, *53*, 262–276.

Galloway, W. E. (2008). Depositional evolution of the Gulf of Mexico sedimentary basin. In K. J. Hsü (Ed.), *Sedimentary basins of the world, Volume 5, The sedimentary basins of the United States and Canada, Miall, A.D., ed*. (pp. 505–549). The Netherlands: Elsevier.

Galloway, W. E., Ganey-Curry, P., & Whiteaker, T. L. (2009). Regional controls from temporal and spatial distribution of continental slope and abyssal plain reservoir systems of the Gulf of Mexico Basin. *AAPG Search and Discovery*, *50226*, 1–26.

Galloway, W. E., Whiteaker, T. L., & Ganey-Curry, P. (2011). History of Cenozoic North American drainage basin evolution, sediment yield, and accumulation in the Gulf of Mexico basin. *Geosphere*, *7*, 938–973. https://doi.org/10.1130/GES00647.1

González, J. L., & Tornqvist, T. E. (2006). Coastal Louisiana in crisis: Subsidence or sea level rise? *Eos, Transactions American Geophysical Union*, *87*, 493. https://doi.org/10.1029/2006EO450001

Gradstein, F. M., Ogg, J. G., Schmitz, M. D., & Ogg, G. M. (2012). *The geologic time scale*. Boston, MA: Elsevier.

Ivins, E. R., Dokka, R. K., & Blom, R. G. (2007). Post-glacial sediment load and subsidence in coastal Louisiana. *Geophysical Research Letters*, *34*, 1–5. https://doi.org/10.1029/2007GL030003

Jankowski, K. L., Törnqvist, T. E., & Fernandes, A. M. (2017). Vulnerability of Louisiana's coastal wetlands to present-day rates of relative sea-level rise. *Nature Communications*, *8*, 14792. https://doi.org/10.1038/ncomms14792

Jones, C. E., An, K., Blom, R. G., Kent, J. D., Ivins, E. R., & Bekaert, D. (2016). Anthropogenic and geologic influences on subsidence in the vicinity of New Orleans, Louisiana. *Journal of Geophysical Research*, *121*, 767–787. https://doi.org/10.1002/2015JB012352

Karegar, M. A., Dixon, T. H., & Malservisi, R. (2015). A three-dimensional surface velocity field for the Mississippi Delta : Implications for coastal restoration and flood potential. *Geology*, *43*, 519–522. https://doi.org/10.1130/G36598.1

Kuecher, G. J., Roberts, H. H., Thompson, M. D., & Matthews, I. (2001). Evidence for active growth faulting in the terrebonne Delta plain, South Louisiana: Implications for wetland loss and the vertical migration of petroleum. *Environmental Geosciences*, *8*, 77–94. https://doi.org/10.1046/j.1526-0984.2001.82001.x

Kulp, M. (2000). *Holocene stratigraphy, history, and subsidence of the Mississippi River Delta region* (p. 283). North central Gulf of Mexico: University of Kentucky.

Love, R., Milne, G. A., Tarasov, L., Engelhart, S. E., & Hijma, M. P. (2016). The contribution of glacial isostatic adjustment to projections of sea-level change along the Atlantic and Gulf coasts of North America. *Earth's Future*, *4*, 440–464. https://doi.org/10.1002/2016EF000363

Martin, J., Cantelli, A., Paola, C., Blum, M., & Wolinsky, M. (2011). Quantitative modeling of the evolution and geometry of Incised Valleys. *Journal of Sedimentary Research*, *81*, 64–79. https://doi.org/10.2110/jsr.2011.5

McBride, B. C., Rowan, M. G., & Weimer, P. (1998). The evolution of allochthonous salt systems, northern Green Canyon and Ewing Bank (offshore Louisiana), northern Gulf of Mexico. *AAPG Bulletin*, *82*, 1013–1036. https://doi.org/10.1306/1D9BC9FD-172D-11D7-8645000102C1865D

McCulloh, R. P., & Heinrich, P. V. (2013). Surface faults of the south Louisiana growth-fault province. *Geological Society of America Special Paper*, *493*, 37–49. https://doi.org/10.1130/2012.2493(03)

McFarlan, E., & LeRoy, D. O. (1988). Subsurface geology of the Late Tertiary and Quaternary deposits, coastal Louisiana and the adjacent continental shelf. *Gulf Coast Association of Geological Societies Transactions*, *38*, 421–433.

McGranahan, G., Balk, D., & Anderson, B. (2007). The rising risks of climate change and human settlements in low elevation coastal zones. *Environment and Urbanization*, *19*, 17–37. https://doi.org/10.1177/0956247807076960

Meckel, T. A. (2008). An attempt to reconcile subsidence rates determined from various techniques in southern Louisiana. *Quaternary Science Reviews*, *27*, 1517–1522. https://doi.org/10.1016/j.quascirev.2008.04.013

Meckel, T. A., ten Brink, U. S., & Williams, S. J. (2006). Current subsidence rates due to compaction of Holocene sediments in southern Louisiana. *Geophysical Research Letters*, *33*, 1–5. https://doi.org/10.1029/2006GL026300

Miller, K. G., Kominz, M. A., Browning, J. V., Wright, J. D., Mountain, G. S., Katz, M. E., … Pekar, S. F. (2005). The Phanerozoic record of global sea-level change. *Science*, *310*, 1293–1298. https://doi.org/10.1126/science.1116412

Miller, K. G., Mountain, G. S., Wright, J. D., & Browning, J. V. (2011). A 180 million year record of sea level and ice volume variations. *Oceanography*, *24*, 40–53. https://doi.org/10.5670/oceanog.2011.26

Milliken, K. T., Anderson, J. B., & Rodriguez, A. B. (2008). A new composite Holocene sea-level curve for the northern Gulf of Mexico. *Response of Upper Gulf Coast Estuaries to Holocene Climate Change and Sea-Level Rise*, *443*, 1–11. https://doi.org/10.1130/2008.2443(01)

Morton, R. A., & Bernier, J. C. (2010). Recent subsidence-rate reductions in the Mississisippi and their geological implications. *Journal of Coastal Research*, *26*, 555–561. https://doi.org/10.2112/JCOASTRES-D-09-00014R1.1

Morton, R. A., Paine, J. G., & Blum, M. D. (2000). Responses of stable Bay-Margin and Barrier-Island systems to Holocene sea-Level highstands, Western Gulf of Mexico. *Journal of Sedimentary Research*, *70*, 478–490. https://doi.org/10.1306/2DC40921-0E47-11D7-8643000102C1865D

Murray, G. E. (1961). *Geology of the Atlantic and Gulf Coastal Provinces of North America* (p. 692). New York, NY: Harper.

Nienhuis, J. H., Törnqvist, T. E., Jankowski, K. L., Fernandes, A. M., & Keogh, M. E. (2017). A new subsidence map for coastal Louisiana. *GSA Today*, *27*, https://doi.org/10.1130/G36598.1

Ogg, J. G., Ogg, G. M., & Gradstein, F. M. (2016). *A concise geologic time scale*. Boston, MA: Elsevier.

Peel, F., Travis, C., & Hossack, J. (1995). Genetic structural provinces and salt tectonics of the Cenozoic offshore US Gulf of Mexico; a preliminary analysis: Salt Tectonics:AAPG Memoir 65, *65*, 153–175.

Penland, S., & Ramsey, K. E. (1990). Relative sea-level rise in Louisiana and the Gulf of Mexico : 1908–1988. *Journal of Coastal Research*, *6*, 323–342.

Pitman, W. C. III, & Golovchenko, X. (1983). The effect of sea-level change on the shelf edge and slope of passive margins. *Society of Economic Paleontologists and Mineralogists Special Publication*, *33*, 41–58.

Roberts, H. H., Bailey, A., & Kuecher, G. J. (1994). Subsidence in the Mississippi River Delta-important influences of valley filling by cyclic deposition, primary consolidation phenomena, and early diagenesis. *Transactions of the Gulf Coast Association of Geological Societies*, *44*, 619–629.

Roberts, H. H., Morton, R. A., & Freeman, A. (2008) A high-resolution seismic assessment of faulting in the Louisiana Coastal Plain. 733–745.

Rodriguez, A. B., Anderson, J. B., Siringan, F. P., & Taviani, M. (2004). Holocene evolution of the east Texas coast and inner continental shelf: Along-strike variability in coastal retreat rates. *Journal of Sedimentary Research*, *74*, 405–421.

Rodriguez, A. B., Anderson, J. B., & Simms, A. R. (2005). Terrace inundation as an autocyclic mechanism for parasequence formation: Galveston Estuary, Texas, U.S.A. *Journal of Sedimentary Research*, *75*(4), 608–620. https://doi.org/10.2110/jsr.2005.050

Rodriguez, A. B., & Meyer, C. T. (2006). Sea-level variation during the Holocene deduced from the morphologic and stratigraphic evolution of Morgan Peninsula, Alabama, U.S.A. *Journal of Sedimentary Research*, *76*, 257–269. https://doi.org/10.2110/jsr.2006.018

Sadler, P. M. (1981). Sediment accumulation rates and the completeness of stratigraphic sections. *Journal of Geology*, *89*, 569–584. https://doi.org/10.1086/628623

Sadler, P. M. (1999). The influence of hiatuses on sediment accumulation rates. In P. Bruns & H. C. Haas (Eds.), *GeoResearch forum: On the determination of sediment accumulation rates* (vol. 5, pp. 15–40). Switzerland: Trans Tech Publications.

Schumer, R., & Jerolmack, D. J. (2009). Real and apparent changes in sediment deposition rates through time. *Journal of Geophysical Research*: Solid: Earth, *114*, 1–12. https://doi.org/10.1029/2009JF001266

Shen, Z., Dawers, N. H., Törnqvist, T. E., Gasparini, N. M., Hijma, M. P., & Mauz, B. (2017). Mechanisms of Late Quaternary fault throw-rate variability along the north central Gulf of Mexico coast: Implications for coastal subsidence. *Basin Research*, *29*, 557–570. https://doi.org/10.1111/bre.12184

Shen, Z., Torrnqvist, T. E., Autin, W. J., Mateo, Z. R. P., Straub, K. M., & Mauz, B. (2012). Rapid and widespread response of the Lower Mississippi River to eustatic forcing during the last glacial-interglacial cycle. *Bulletin of the Geological Society of America*, *124*, 690–704. https://doi.org/10.1130/B30449.1

Shinkle, K., & Dokka, R. (2004) Rates of vertical displacement at benchmarks in the lower Mississippi valley and the Northern Gulf Coast, *in* NOAA Technical Report NGS 50, *50*, 135.

Simms, A. R., Lambeck, K., Purcell, A., Anderson, J. B., & Rodriguez, A. B. (2007). Sea-level history of the Gulf of Mexico since the Last Glacial Maximum with implications for the melting of the Laurentide Ice Sheet. *Quaternary Science Reviews*, *26*, 920–940. https://doi.org/10.1016/j.quascirev.2007.01.001

Spurr, J. E. (1897). The measurement of faults. *Journal of Geology*, *5*, 723–729. https://doi.org/10.1086/607929

Stephens, B. P. (2010) Basement controls on subsurface geologic patterns and near-surface geology across the Northern Gulf of Mexico: A Deeper Perspective on Coastal Louisiana: Search and Discovery. *30129*, 1–12.

Straub, K. M., Paola, C., Mohrig, D., Wolinsky, M. A., & George, T. (2009). Compensational stacking of channelized sedimentary deposits. *Journal of Sedimentary Research*, *79*, 673–688. https://doi.org/10.2110/jsr.2009.070

Syvitski, J. P. M. (2008). Deltas at risk. *Sustainability Science*, *3*, 23–32. https://doi.org/10.1007/s11625-008-0043-3

Syvitski, J. P. M., & Milliman, J. D. (2007). Geology. Geography, and humans battle for dominance over the delivery of fluvial sediment to the coastal Ocean. *Journal of Geology*, *115*, 1–19. https://doi.org/10.1086/509246

Syvitski, J. P. M., & Saito, Y. (2007). Morphodynamics of deltas under the influence of humans. *Global and Planetary Change*, *57*, 261–282. https://doi.org/10.1016/j.gloplacha.2006.12.001

Törnqvist, T. E., Bick, S. J., van der Borg, K., & de Jong, A. F. M. (2006). How stable is the Mississippi Delta? *Geology*, *34*, 697–700. https://doi.org/10.1130/G22624.1

Törnqvist, T. E., González, J. L., Newsom, L. A., van der Borg, K., de Jong, A. F. M., & Kurnik, C. W. (2004). Deciphering Holocene sea-level history on the U.S. Gulf Coast: A high-resolution record from the Mississippi Delta. *Bulletin of the Geological Society of America*, *116*, 1026–1039. https://doi.org/10.1130/B2525478.1

Törnqvist, T. E., Wallace, D. J., Storms, J. E. A., Wallinga, J., van Dam, R. L., Blaauw, M., … Snijders, E. M. A. (2008). Mississippi Delta subsidence primarily caused by compaction of Holocene strata. *Nature Geoscience*, *1*, 173–176. https://doi.org/10.1038/ngeo129

Watts, A. B., Zhong, S. J., & Hunter, J. (2013). The behavior of the Lithosphere on Seismic to Geologic Timescales. *Annual Review of Earth and Planetary Sciences*, *41*, 443–468. https://doi.org/10.1146/annurev-earth-042711-105457

Wolstencroft, M., Shen, Z., Törnqvist, T. E., Milne, G. A., & Kulp, M. (2014). Understanding subsidence in the Mississippi Delta region due to sediment, ice, and ocean loading: Insights from geophysical modeling. *Journal of Geophysical Research*: Solid: Earth, *119*, 3838–3856. https://doi.org/10.1002/2013JB010928

Woodbury, H. O., Murray, I. B. Jr, Pickford, P. J., & Akers, W. H. (1973). Pliocene and Pleistocene depocenters, outer continental shelf, Louisiana and Texas. *American Association of Petroleum Geologists*, *57*, 2428–2439.

Yu, S. Y., Törnqvist, T. E., & Hu, P. (2012). Quantifying Holocene lithospheric subsidence rates underneath the Mississippi Delta. *Earth and Planetary Science Letters*, *331–332*, 21–30. https://doi.org/10.1016/j.epsl.2012.02.021

Yuill, B., Lavoie, D., & Reed, D. J. (2009). Understanding subsidence process in coastal Louisiana. *Journal of Coastal Research*, *54*, 23–36. https://doi.org/10.2112/SI54-012.1

SUPPORTING INFORMATION

Additional supporting information may be found online in the Supporting Information section at the end of the article.

How to cite this article: Frederick BC, Blum M, Fillon R, Roberts H. Resolving the contributing factors to Mississippi Delta subsidence: Past and Present. *Basin Res*. 2018;00:1–20. https://doi.org/10.1111/bre.12314